Research Square

Preprints are preliminary reports that have not undergone peer review.
They should not be considered conclusive, used to inform clinical practice,
or referenced by the media as validated information.

Placental iron dysregulation links maternal obesity with fetal and offspring iron deficiency

Jonas Zaugg

jonas.zaugg@uzh.ch

University of Cambridge Department of Physiology: University of Cambridge Department of Physiology Development and Neuroscience https://orcid.org/0000-0002-3153-2806

Samantha C Lean

University of Manchester Developmental Biomedicine Research Group: The University of Manchester Faculty of Biology Medicine and Health

Megan Vickers

Warwick Medical School: University of Warwick Medical School

Alejandro A Candia

University of Cambridge Department of Physiology: University of Cambridge Department of Physiology Development and Neuroscience

Ivona Bečeheli

Ruder Boskovic Institute: Institut Ruder Boskovic

Edina Gulacsi

University of Cambridge Department of Physiology: University of Cambridge Department of Physiology Development and Neuroscience

Amanda N Sferruzzi-Perri

University of Cambridge Department of Physiology: University of Cambridge Department of Physiology Development and Neuroscience https://orcid.org/0000-0002-4931-4233

Research Article

Keywords: Maternal obesity, placenta, iron transport, ferroptosis, fetal growth restriction, developmental programming

Posted Date: November 25th, 2026

DOI: https://doi.org/10.21203/rs.3.rs-11613579/v1

License: This work is licensed under a Creative Commons Attribution 4.0 International License.
Read Full License

Placental iron dysregulation links maternal obesity with fetal and offspring iron deficiency

Jonas Zaugg[1,2], Samantha C Lean[1,2], Megan Vickers[1,2], Alejandro A Candia[1,3], Ivona Bečeheli[1,2,4], Edina Gulacsi[1], Amanda N Sferruzzi-Perri[1,2,^]

[1] Department of Physiology, Development and Neuroscience, University of Cambridge, UK

[2] Loke Centre for Trophoblast Research, Department of Physiology, Development and Neuroscience, University of Cambridge, Cambridge, UK

[3] Department for the Woman and Newborn Health Promotion, Universidad de Chile, Santiago, Chile

[4] Division of Molecular Biology, Ruđer Bošković Institute, Zagreb, Croatia

^ Correspondence:

Prof. Amanda N. Sferruzzi-Perri
University of Cambridge
Department of Physiology, Development and Neuroscience
Downing Street
CB2 3EG, Cambridge, UK

Phone: +44 1223 333807
E-Mail: ans48@cam.ac.uk

Running title:
Placental iron handling links maternal obesity and developmental programming

Keywords:
Maternal obesity; placenta; iron transport; ferroptosis; fetal growth restriction; developmental programming

1.1 Abstract

Maternal obesity is associated with placental dysfunction and adverse offspring outcomes, but the contribution of placental micronutrient transport remains unclear. We investigated whether pre-gestational obesity disrupts placental iron handling and ferroptosis-associated pathways, limiting fetal iron acquisition and contributing to developmental programming.

Female mice were fed a control or obesogenic diet before and during pregnancy. Maternal, placental, fetal, and adult offspring iron status, iron deposition, and expression of iron homeostasis- and ferroptosis-related genes were assessed. Placental transcriptomics were integrated with developmental single-nucleus RNA-sequencing data.

Maternal obesity preserved maternal iron status but reduced placental iron deposition, placental iron transport capacity, fetal circulating iron concentrations, and iron accumulation in fetal liver and brain. These changes were accompanied by placental transcriptomic remodeling characterized by increased *Acsl4* expression and reduced antioxidant and anti-ferroptotic pathways. Single-nucleus analyses identified syncytiotrophoblasts as the cellular hub coordinating iron transport and ferroptosis-associated pathways. Maternal obesity also restricted placental and fetal growth. Although circulating and hepatic iron status largely normalized in adult offspring, brain iron deficiency persisted with alterations in cerebral ferroptosis-associated gene networks.

Maternal obesity uncouples maternal and fetal iron homeostasis through placental iron dysregulation, linking impaired fetal iron acquisition with fetal growth restriction and offspring brain iron deficiency.

Graphical abstract

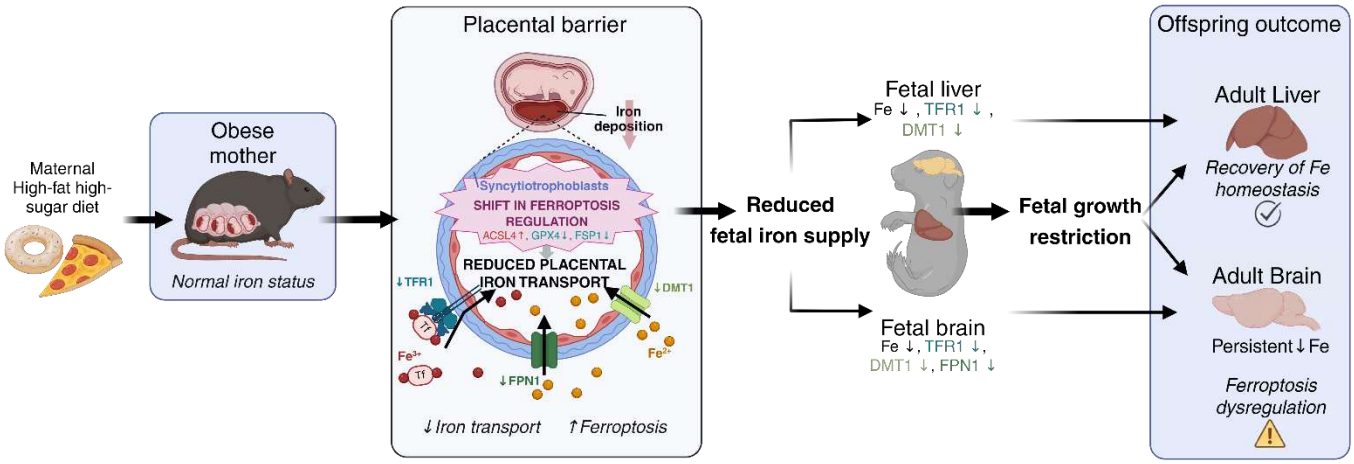


Figure 1 Graphical Abstract

A maternal obesogenic high-fat, high-sugar diet is associated with placental iron dysregulation, fetal growth restriction, and persistent offspring brain iron deficiency. In the placenta, altered expression of ferroptosis-related genes (*Acsl4*, *Gpx4*, and *Fsp1*) coincides with reduced iron transport and dysregulation of iron deposition and transporters including transferrin receptor 1 (*Tfr1*), divalent metal transporter 1 (*Dmt1*), and ferroportin (*Fpn1*). These placental alterations occur alongside reduced fetal liver and brain iron content and fetal growth restriction. Postnatally, offspring show divergent outcomes, with normalization of iron homeostasis in the adult liver, but persistent brain iron deficiency and ferroptosis-related dysregulation. These findings identify the placenta as a key site associated with maternal obesity, altered iron handling, and organ-specific programming of offspring iron homeostasis.

Genes: ACSL4, acyl-CoA synthetase long-chain family member 4; GPX4, glutathione peroxidase 4; FSP1, ferroptosis suppressor protein 1; TFR1, transferrin receptor 1; DMT1, divalent metal transporter 1; FPN1, ferroportin 1; FGR, fetal growth restriction; Fe, iron.

2 Introduction

Maternal obesity is one of the most prevalent metabolic complications of pregnancy worldwide and is associated with increased risks of placental dysfunction, abnormal fetal growth, and adverse long-term offspring health outcomes [1, 2]. Both clinical and experimental animal studies have demonstrated that maternal obesity alters placental development and nutrient allocation to the fetus, thereby contributing to developmental programming of later-life metabolic, cardiovascular, and neurological disease [3–5]. Importantly, these adverse outcomes frequently occur despite apparently adequate or excess maternal nutrient availability, suggesting that placental dysfunction is a critical intermediate linking maternal metabolic disturbances with impaired fetal development [6]. Although most studies have focused on obesity-induced alterations in placental glucose, amino acid and lipid transport, fetal development also depends on the efficient placental transfer of essential micronutrients. Whether maternal obesity disrupts placental micronutrient transport remains largely unknown and represents a significant knowledge gap.

Among the micronutrients supplied by the placenta, iron is particularly important because it can only reach the fetus via placental transfer from the maternal circulation. Fetal iron requirements increase substantially during late gestation to support rapid growth, oxygen transport, anabolic processes, mitochondrial function, and the establishment of iron stores required for postnatal development [7, 8]. Rapidly developing organs, particularly the liver and brain are especially dependent on adequate fetal iron supply. In both humans and mice, placental iron transport is mediated by a coordinated network of uptake, intracellular trafficking, storage, and export pathways involving transferrin receptor 1 (TFR1), divalent metal transporter 1 (DMT1), ferroportin (FPN1), and their regulation by iron-regulatory proteins, including hepcidin (HAMP), Iron regulatory protein 2 (IRP2) and Hypoxia-inducible factor 1-alpha (HIF1A) [7, 9, 10]. Disruption of this tightly controlled network impairs fetal iron accretion and has been linked to fetal growth restriction, altered organ development, and long-term neurodevelopmental abnormalities [8, 11]. However, whether maternal obesity affects placental iron transport and consequently limits fetal iron acquisition remains poorly understood.

Accumulating clinical and experimental evidence indicates that maternal obesity disrupts iron homeostasis in both the mother and fetus, highlighting placental iron transport as a biologically plausible mechanism [12, 13]. Maternal overweight and obesity have been associated with reduced maternal iron stores and altered iron parameters, while fetal iron indices and neonatal ferritin concentrations are also lower in infants of mothers with obesity [14–17]. These observations suggest that maternal obesity may limit iron availability for placental transfer and fetal iron accretion.

Placental iron delivery depends on transferrin receptor 1 (TfR1)-mediated uptake of diferric transferrin by the syncytiotrophoblast, endosomal iron release, and ferroportin (FPN1)-mediated export into the fetal circulation, followed by loading onto fetal transferrin [18–21]. This pathway is regulated by maternal hepcidin, which is normally suppressed during pregnancy to promote iron mobilization and fetal supply [18, 21, 22]. In obesity, however, low-grade inflammation and insulin resistance may elevate hepcidin through interleukin-6 (IL-6)/ c-reactive peptide (CRP)-mediated JAK–STAT3 signaling, thereby reducing iron absorption, mobilization, and potentially placental transfer [22, 23]. Experimental evidence supports the importance of this mechanism:

maternal, rather than embryonic, hepcidin determines embryo and placental iron endowment in mice, and modest maternal hepcidin elevation can cause fetal anemia, tissue iron deficiency, and reduced fetal weight even without overt maternal anemia [12].

Direct evidence from an obesogenic high-fat, high-sugar diet pregnant mouse model further demonstrates impaired placental iron handling, including reduced placental iron transfer capacity, TfR1 expression, and iron deposition, together with oxidative stress and ERK, p38 MAPK, and JNK signaling activation [6]. Importantly, these alterations were gestation-dependent, as early reductions in TfR1 and ERK2 signaling accompanied lower fetal weight, whereas later timepoints showed persistent reductions in placental iron content and transporter genes including *Dmt1*, *Zip14*, and *Fpn1*, despite normalization of fetal weight in obesogenic high-fat, high-sugar diet fed pregnant mice [6]. Clinical studies in women with gestational diabetes and elevated body mass index (BMI) similarly report dysregulated placental iron transporter expression, although findings are heterogeneous and may reflect compensatory responses to fetal iron deficiency [13].

Understanding placental iron transport is also important because iron is highly reactive and a central regulator of oxidative stress pathways that influence essential cellular functions. Iron homeostasis is closely linked with ferroptosis, an iron-dependent form of regulated cell death driven by excess iron, lipid peroxidation and oxidative membrane damage. Recent studies have implicated ferroptosis in several placental disorders, including fetal growth restriction, preeclampsia, gestational diabetes, and maternal obesity [24–26]. Maintenance of placental transport function therefore requires robust antioxidant and anti-ferroptotic defense systems, including GPX4, FSP1, glutathione synthesis pathways, and intracellular iron-buffering proteins [27]. In mice, we recently demonstrated that obesity restricted to pregnancy was sufficient to induce oxidative stress and coordinated alterations in placental iron homeostasis and ferroptosis-associated pathways, suggesting impaired placental iron handling as a potential mechanism linking maternal obesity with fetal growth abnormalities [6]. However, the cellular localization of iron transport and ferroptosis pathways within the placental exchange barrier during pregnancy remains poorly defined. Furthermore, it is unknown whether pre-existing diet-induced maternal obesity alters these pathways in the placenta or may influence fetal iron accretion, fetal growth and long-term offspring iron homeostasis.

We hypothesized that pre-existing diet-induced maternal obesity disrupts placental iron transport and promotes a pro-ferroptotic placental environment, thereby impairing fetal iron delivery, restricting fetal growth and inducing persistent alterations in offspring iron homeostasis. To test this hypothesis, we first analyzed a developmental single-nucleus RNA-sequencing atlas to characterize the cellular localization and developmental dynamics of iron-related genes in the mouse placenta. We then employed an established mouse model of pre-existing maternal obesity induced by a high fat, high sugar (HFHS) diet [4, 5, 28] to investigate placental iron transport and fetal iron acquisition. Placental bulk RNA-sequencing was used to identify obesity-associated transcriptomic changes in iron homeostasis and ferroptosis pathways and to examine their relationships with maternal metabolic characteristics during pregnancy. Finally, we assessed iron accretion in the fetal liver and brain and evaluated whether alterations in iron homeostasis persisted in adulthood in offspring exposed to maternal obesity.

3 Material and Methods

3.1 Reagents

All chemicals and reagents were purchased from Sigma Aldrich unless otherwise stated.

3.2 Single-nucleus RNA sequencing analysis

Single-nucleus RNA sequencing (snRNA-seq) data were obtained from the mouse placental developmental atlas generated by Marsh and Blelloch (2020) (GEO accession GSE152248). Analyses were performed in Seurat (v5.3.0) using integrated datasets spanning embryonic day (E)9.5, E10.5, E12.5, and E14.5 of placental development. Two Seurat objects were used: an integrated object containing all placental nuclei and a trophoblast-focused object.

For trophoblast-specific analysis, the AllStages_TrophoblastNuclei object was employed to characterize expression patterns within the placental barrier and develop a comprehensive working model of placental iron transport. Major trophoblast populations included labyrinth trophoblast progenitors (LaTP), syncytiotrophoblast layer I (SynTI), syncytiotrophoblast layer II (SynTII), sinusoidal trophoblast giant cells (S-TGC), spongiotrophoblasts (SpT), glycogen cells, and junctional zone progenitors (JzP), focusing on mature trophoblast cell types. The AllStages_AllNuclei object enabled visualization of iron homeostasis and ferroptosis marker gene expression across diverse placental cell populations at E14.5, such as non-trophoblast populations included endothelial cells, fetal mesenchyme, decidual stromal cells, hematopoietic populations, and macrophages.

Expression patterns of genes involved in iron transport, iron regulation, intracellular iron handling, oxidative stress, and ferroptosis were visualized using UMAP projections and dot plots. Developmental gene-expression dynamics were assessed using linear regression across E9.5–E14.5. Significant positive and negative trends were summarized graphically as directional arrows. This approach was used to identify monotonic developmental changes and avoided capture of transient or biphasic expression patterns.

3.3 Maternal obesity model

All animal procedures were conducted in accordance with the UK Home Office Animals (Scientific Procedures) Act 1986 and were approved by the University of Cambridge Animal Welfare and Ethical Review Board.

An established mouse model of pre-gestational diet-induced obesity was used as previously described [4, 5, 28]. Female C57BL/6J mice were purchased from Inotiv formerly known as Envigo RMS (UK) at 6 weeks of age and randomly assigned to either a standard chow diet (RM3; Special Diet Services, Witham, UK) or an obesogenic HFHS diet. The HFHS diet consisted of a high-fat pellet diet (D12451; Research Diets Inc., Denmark) supplemented with condensed milk (Carnation, Nestlé, Gatwick, UK) at a ratio of 1.5:1. Detailed dietary composition and validation of this model have been reported previously [5, 28].

To establish obesity and confirm fertility, females underwent an initial breeding cycle while maintained on their allocated diets. Following completion of lactation, dams remained on their respective diets and were remated with chow-fed C57BL/6J males seven days after weaning of the first litter (Figure 1A). Consequently, females were exposed to the allocated diets for approximately 9 weeks prior to conception of the experimental pregnancy and remained on the same diet throughout gestation and lactation [5, 28].

The day of copulatory plug detection was designated embryonic day (E)0.5. Maternal body weight was monitored throughout pregnancy. Maternal adiposity was assessed using time-domain nuclear magnetic resonance (TD-NMR; LF50H Minispec, Bruker, Coventry, UK) immediately before mating and again at E17.5. Food consumption was recorded weekly throughout gestation by total food consumption per cage divided by the total number of mice in the cage.

3.4 Tissue collection

For assessment of maternal-fetal outcomes, at E18.5 dams were anaesthetized (Fentanyl (Fentadon, Dechra Vetinary Products UK), Midazolam (Roche) and Ketamine (Ketavet, Zoetis, UK) diluted in water, injected i.p. with 10µl/g) and cardiac blood was collected. Dams were the euthanized by cervical dislocation and maternal organs, placentae, fetal blood, fetal liver, and fetal brain tissues were collected. For assessment of long-term offspring outcomes, a separate cohort of dams was allowed to deliver naturally. Litters were standardized to three males and three females on postnatal day 3. As shown in Figure 3A, all offspring were transferred at weaning to standard chow diet irrespective of maternal dietary group and maintained until 14 weeks of age, when they were anaesthetized, blood taken, "Schedule 1" killed and tissues collected for analysis. Maternal and offspring blood was collected into EDTA tubes and centrifuged to obtain plasma, with additional sample of fetal blood collected to obtain fetal serum. Fetal sex was determined by visual inspection and confirmed through PCR amplification of the Sry gene using tail-derived DNA.

Maternal analyses were performed in n=20 control dams and n=22 dams exposed to maternal obesity. For fetal analyses, one male and one female fetus per litter were selected for blood iron measurements, tissue iron quantification, and RT-qPCR analyses. Histological analyses were performed on n=5–7 placentas per sex and dietary group including 5–6 litters. Placental RNA sequencing was performed on n=6 placental labyrinth samples per sex and dietary group across different litters. Postnatal studies were conducted in n=7–8 offspring per sex and maternal diet group across multiple litters. Unless otherwise stated, the litter was considered the experimental unit for fetal/offspring analyses.

3.5 Assessment of blood iron status

Plasma and serum iron concentrations were measured using the QuantiChrom™ Iron Assay Kit (DIFE-250, BioAssay Systems, Hayward, CA, USA) according to the manufacturer's instructions. Absorbance was measured at 590 nm using a V_{Max} Kinetic ELISA Microplate Reader (Molecular Devices LLC, USA), and iron concentrations were calculated from standard curves generated using supplied iron standards. Total iron-binding capacity (TIBC) and transferrin saturation were subsequently calculated from circulating

iron concentrations. Circulating hepcidin concentrations were quantified using a Mouse HAMP ELISA Kit (OKEH01408, Aviva Systems Biology, San Diego, CA, USA) according to the manufacturer's instructions. Hematocrit was measured after collecting whole blood from mice using heparinized capillary tubes centrifuged at 12,000 × g for 5 min using a micro-hematocrit centrifuge (Hawksley, UK). Packed cell volume was expressed as a percentage of total blood volume. Placental iron transport capacity was calculated as the ratio of fetal serum iron concentration to maternal plasma iron concentration as follows:

$$Placental\ iron\ transport\ capacity\ = fetal\ serum\ iron\ /maternal\ plasma\ iron$$

Lower values indicated impaired fetal acquisition of maternal iron.

3.6 Tissue iron quantification

Iron concentrations in fetal and adult liver and brain tissues were determined using an adapted ferrozine-based colorimetric assay as previously described [6, 29]. Tissues were homogenized in RIPA buffer and protein concentrations determined using a bicinchoninic acid (BCA) assay (Thermo Fisher Scientific, USA). Equal volumes of 100 mM NaOH were added to lysates prior to iron release using an acidic oxidation reagent consisting of 1.4 M HCl and 4.5% (w/v) potassium permanganate. Samples were incubated for 2 h at 60°C. Following cooling, iron detection reagent containing 6.5 mM ferrozine; 6.5 mM neocuproine; 2.5 M ammonium acetate; 1 M ascorbic acid was added in a 1:10 ratio (v/v) and samples incubated for 30 min at room temperature. Absorbance was measured at 550 nm using a microplate reader. Iron concentrations were interpolated from $FeCl_3$ standards and normalized to protein concentration. Samples were measured in duplicate. Results are reported as pmol iron/mg tissue protein. Total organ iron content was calculated from tissue iron concentration and organ weight.

3.7 Histological assessment of placental iron deposition

Placental halves fixed in 4% paraformaldehyde were paraffin embedded and sectioned at 5 μm as previously described [30]. Iron deposition was visualized using Prussian Blue staining. In brief, placenta sections were stained with 10% (w/w) Prussian blue ($K_4Fe(CN)_6$ x $3H_2O$) for 5 min and the mixture of 10% (w/w) Prussian blue and 20% HCl (1 : 1) for 30 min and finally counterstained with nuclear fast red for 5 min. Sections were scanned using a NanoZoomer S210 Digital Slide Scanner (Hamamatsu Photonics, Japan). Images were analyzed using QuPath and ImageJ [31]. Cross-sections were subdivided into decidua, junctional zone, and labyrinth zone compartments. Iron-positive tissue areas were identified using threshold-based color segmentation and normalized to total tissue area within each placental compartment.

3.8 RNA extraction and quantitative real-time PCR

Total RNA was extracted from placental, fetal liver, fetal brain, adult liver, and adult brain tissues using the mirVana™ miRNA Isolation Kit (AM1560, Thermo Fisher Scientific, USA). RNA concentration and purity were assessed spectrophotometrically, and 2.5 µg RNA was reverse-transcribed using the High-Capacity cDNA Reverse Transcription Kit (Applied Biosystems, USA). Quantitative real-time PCR (RT-qPCR) was performed using GoTaq® qPCR Master Mix (A6001, Promega, USA) on a LightCycler® 480 Instrument II (Roche Diagnostics, Switzerland). Reactions were conducted in duplicate in 384-well plates. Amplification specificity was verified by melting curve analysis. Gene expression was quantified using the -ΔCt method and normalized to the geometric mean of four reference genes (*Ywhaz*, *Gapdh*, *Ubi*, and *Tbp*). Reference gene stability was assessed prior to analysis using geNorm [32] , NormFinder [33] , and BestKeeper [34] algorithms to compare and rank the tested candidate reference genes. Relative expression values were calculated relative to the corresponding control group mean. Primer sequences are provided in Supplementary Table 1.

Supplemental Table 1: Primer list

Gene name	NCBI Accession	Forward Primer [5'-3']	Reverse Primer [5'-3']	Product Length (bp)
Tfr1	NM_011638.4 (Var 1) NM_001357298.1 (Var 2)	TGGTGACCATAGTGCAGTCAA	TGGGCATTTGCAACCTTTTCT	217
Dmt1	NM_001146161.1 (Var 1) +IRE NM_008732.2 (Var 2) -IRE NM_001356952.1 (Var 3)	GCAGGAGGTTGACTGGGTC	TGCTCTTAGAATAGGATTCGGCT	96
Zip8	NM_001135150.1 (Var 1) NM_001135149.1 (Var 2) NM_026228.5 (Var 3)	GGGACTAGCTTTCGGCATTT	GCATGTCGTTCATCTCTGGA	122
Zip14	NM_001135151.1 (Var 1) NM_001135152.1 (Var 2) NM_144808.4 (Var 3)	GGACCGCTATGGAAAGAATGAC	CTCACTCGCCCCGATCTG	196
Fpn1	NM_016917.2	TGCAGGAGTCATTGCTGCTAG	TGGAGTTCTGCACACCATTGAT	119
Heph	NM_010417.2 (Var 1) NM_181273.4 (Var 2) NM_001159627.1 (Var 3) NM_001159628.1 (Var 4)	GAATTTTGCGAGCCGACCTT	TCATCCGCTTTCAGATACCC	111
Cp	(10 gene variants) NM_001409646.1 NM_007752.4 …	TCTTGGAATCCTAGGTCCTGTC	TGAGGAGCGACCTGGTG	160
Zp	NM_001164797.1	CTACGACAAGGATTCGGAAGGAG	GGGCATCAATGTGTGAGTGG	182
Hamp	NM_032541.2	AGGGCAGACATTGCGATACC	GCAACAGATACCACACTGGGA	111
Hfe	NM_010424.5 (Var 1) NM_001347493.1 (Var 2)	CAAGATCCGTGCCAAACAGAAC	GGCGAGTCACTTTCACCAAAG	128
Irp1 (Aco1)	NM_007386.2	AGCCTTTGGGAGTGAACGC	GATGACATGCTGCCTTTCCAC	98
Irp2	NM_022655.3	CCGGGGATCGTGTGATTCTG	ACACTGTCTCAGGTTCAGGC	122
Gss	NM_008180.2 (Var 1) NM_001291111.1 (Var 2)	TAACGGCGTGCGGAGTTT	GTCCTTTTTGATGGTGCTAGACAG	210
Gclc	NM_010295.2	GATGCCAACGAGTCTGACCA	ACCTTGGACAGCGGAATGAG	227
Pla2g6	(15 gene variants) NM_016915.4 NM_001199023.1 NM_001199024.1 NM_001199025.1 …	GAGCAGAGGGGCAGGCT	CCAGTTGGAAGAGCCGGAAG	265
Gpx4	NM_008162.4 (Var 1) NM_001037741.4 (Var 2) NM_001367995.1 (Var 3)	GCACGAATTCTCAGCCAAGG	GATGCACACGAAACCCCTGT	73
Aifm2 (Fsp1)	NM_153779.2 (Var 1)	ACCGCAGTGCATTTGAGAGT	GGCCTCTGCTTCATGGAGTT	196

	NM_178058.4 (var 2) NM_001039194.3 (Var 3) NM_001284300.1 (Var 4)			
Acsl4	NM_207625.2 (Var 1) NM_019477.3 (Var 2) NM_001033600.1 (Var 3)	GGAAAGCAAACTGAAGGCGG	CCCTCAGGGTACTCTGCTCT	99
xCT (Slc7a11)	NM_011990.2	ACTGCCATGGTCAGAAAGCC	GCATAGGACAGGGCTCCAAAAAG	299
Alox15	NM_009660.3	AAGGTGATGAGCACAGGTGG	CCCACCACGTACCGATTCAT	185
FtMt	NM_026286.3	CAAGCACATCAGCTCTGCAC	TCCAGGTTGATTTGGCGGTT	222
Pcbp2	(27 gene variants) NM_001103165.2 NM_001103166.2 ...	GGTTTGGATGCATCTGCTCA	TTGATTTTGGCGCCTTGACG	95
Ywhaz	(5 gene variants) NM_011740.3 NM_001253805.1 …	TTGATCCCCAATGCTTCGC	CAGCAACCTCGGCCAAGTAA	88
Gapdh	(8 gene variants) NM_001289726.1 NM_008084.4 …	GAAGGGCTCATGACCACAGTC	CACGTCAGATCCACGACGG	227
Ubi	NM_019639.4	CCCACACAAAGCCCCTCAAT	AAGATCTGCATCGTCTCTCTCAC	70
Tbp	NM_013684.3	CCCTATCACTCCTGCCACAC	CTGCAGCAAATCGCTTGGG	158

Legend: All known gene variants were detected and amplified the same sequence according to melt curve analyses performed for each measurement.

3.9 Placental labyrinth zone RNA sequencing analysis

RNA sequencing data of dissected placental labyrinth zones from control and dams exposed to maternal obesity were obtained from a previously published dataset (GEO accession GSE262011; [5]). Raw count data were re-analyzed in R (v4.4.1) to examine genes involved in iron homeostasis and ferroptosis. Expression values were scaled as Z-scores to facilitate comparison across samples. Heatmaps were generated using the ComplexHeatmap package with hierarchical clustering based on Pearson correlation distance. Differentially expressed genes associated with iron metabolism and ferroptosis were extracted for downstream visualization and statistical analyses.

3.10 Morphometric calculations

Placental efficiency was calculated as the fetal-to-placental weight ratio. Relative organ weights were calculated as organ weight normalized to body weight and expressed as a percentage of total body weight. Total liver and brain iron content were calculated from tissue iron concentration and corresponding organ weight.

3.11 Statistical analyses

Statistical analyses were performed using GraphPad Prism (v10.4.2) and R (v4.4.1). Data distribution was assessed using Shapiro-Wilk tests. Maternal biometric outcomes were analyzed using unpaired Student's t-tests or Mann-Whitney tests where appropriate. Longitudinal measurements of maternal food intake, energy intake, and iron intake were analyzed using mixed-effects models with maternal diet, gestational age, and the diet × gestational age interaction included as fixed effects. Fetal outcomes were generally analyzed using linear mixed-effects models including maternal diet, fetal sex, and their interaction as fixed effects while transcript

abundance data were analyzed by two-way ANOVA with maternal diet and fetal sex as factors, followed by Fisher's least significant difference (LSD) post hoc test. Fisher's LSD was selected over more conservative corrections to maximize statistical power for these localized comparisons within our 2 group × 2 sex factorial design, ensuring optimal sensitivity for detecting target mRNA expression changes via RT-qPCR.

Whilst litter size at E18.5 was not different between groups, litter size was reduced in dams fed the HFHS diet shortly after birth compared to controls [28]. Hence, litter size was included as a covariate in present analyses, and dam identity was included as a random effect. Adult offspring outcomes were analyzed using linear models containing maternal diet, offspring sex, and their interaction as fixed effects. Estimated marginal means were calculated using the emmeans package and post hoc comparisons were adjusted using Tukey correction where appropriate. Data are presented as mean ± SEM unless otherwise stated. Statistical significance was accepted at $P < 0.05$.

4 Results

4.1 Single-nucleus RNA sequencing identifies syncytiotrophoblasts as the principal cellular site for placental iron handling and regulation of ferroptosis-associated pathways

We first defined the cellular localization of iron homeostasis pathways within the placenta, by anlyzing a developmental mouse placental single-nucleus RNA sequencing atlas (Marsh and Blelloch 2020), comprising more than 119,000 nuclei collected between E9.5 and E14.5. Unsupervised clustering identified major placental cell populations present at E14.5, including trophoblast, stromal, vascular and hematopoietic lineages (Fig. 2A). Further analysis of the trophoblast population resolved as labyrinth trophoblast progenitors (LaTP), syncytiotrophoblast layer I (SynTI), syncytiotrophoblast layer II (SynTII), sinusoidal trophoblast giant cells (S-TGC), spongiotrophoblasts (SpT), glycogen cells and junctional zone progenitors (JzP1 and JzP2) (Fig. 2B).

Analysis of iron homeostasis genes across non-trophoblast populations revealed distinct cell-type-specific signatures (Fig. 2C). Decidual stromal cells exhibited prominent expression of genes involved in iron uptake and storage, including *Tfrc*, *Fth1* and *Ftl1*, whereas erythrocytes were enriched for iron-utilization pathways. Endothelial, mesenchymal and immune populations displayed more restricted expression of iron homeostasis genes, suggesting that the trophoblast populations at the materno-fetal interface possess more extensive molecular machinery for iron handling (Fig. 2C).

Within the trophoblast compartment, expression of iron transport machinery was concentrated at the placental exchange barrier (Fig. 2D). The syncytiotrophoblast layers (SynTI and SynTII) exhibited the broadest expression of genes involved in iron uptake, intracellular trafficking and export, including *Tfrc*, *Slc39a8*, *Slc11a2*, *Slc40a1*, *Slc25a37*, *Flvcr2* and *Slc48a1*. The spongiotrophoblasts (SpTs), which lay between the placental exchange region and decidua highly expressed heme-iron handling genes, such as *Lrp1*, *Flvcr2* and a few anti-ferroptotic genes. S-TGCs, which are directly exposed to maternal blood, expressed

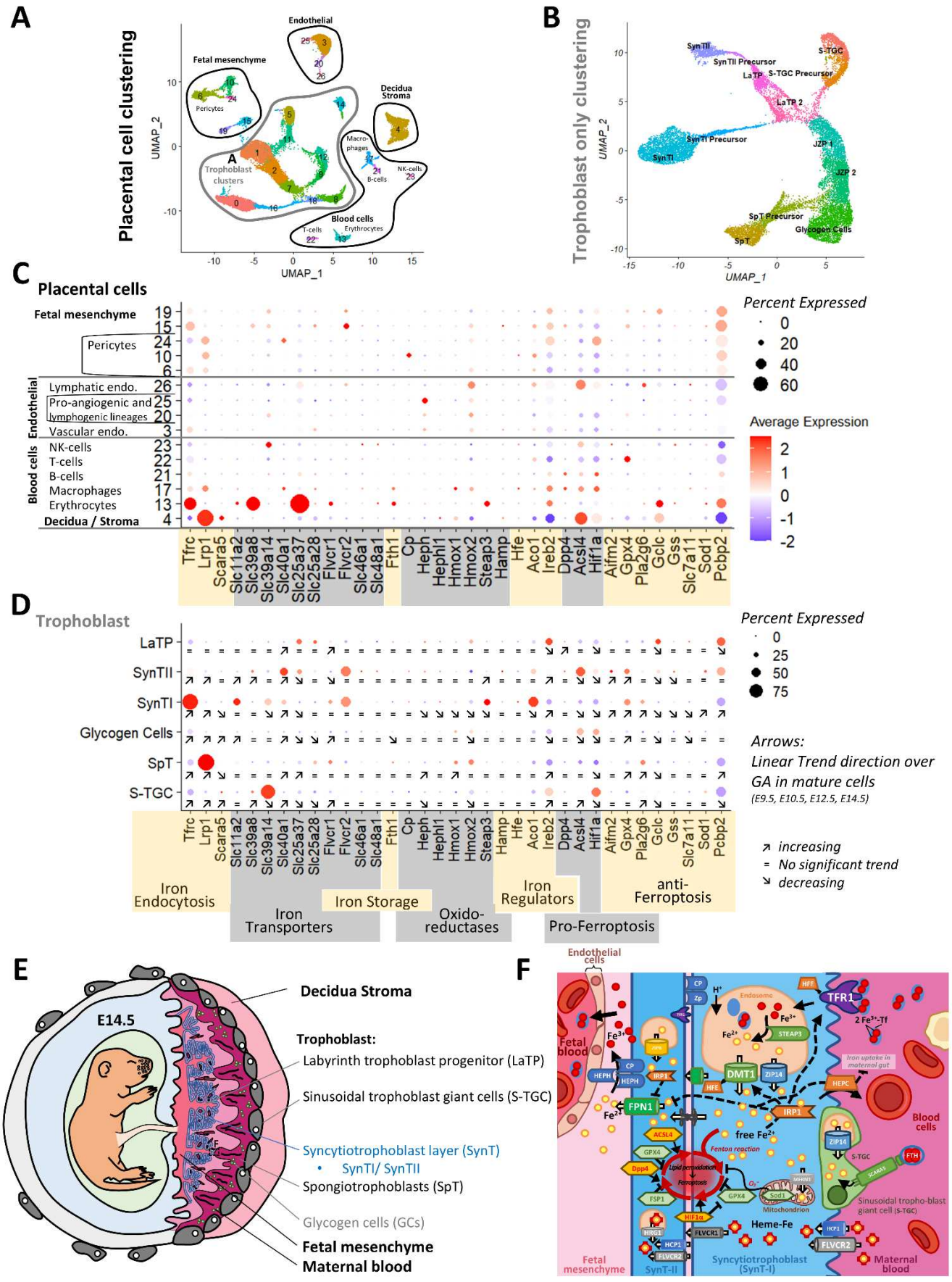
selected iron-handling and stress-response genes, including *Slc39a14* and *Hif1a*, suggesting a role in iron acquisition and cellular adaptation at the maternal interface (Fig. 2D). In contrast, glycogen cells expressed relatively few iron transport genes.

Genes involved in intracellular iron storage and regulation were distributed across multiple trophoblast populations. *Fth1* and *Pcbp2* were broadly expressed, consistent with roles in intracellular iron buffering, while *Hamp*, *Aco1* and *Ireb2* were detected across several lineages, suggesting widespread local regulation of iron availability (Fig. 2D). A more spatially organized expression pattern was observed for oxidoreductases and hem-processing genes. For example, S-TGCs exhibited robust expression of *Cp*, *Hmox1* and *Hmox2*, consistent with iron mobilization and hem-iron processing at the maternal blood interface. The syncytiotrophoblast layers showed prominent expression of *Heph* together with the core transport machinery (*Tfrc*, *Slc11a2* and *Slc40a1*), supporting sequential uptake, intracellular movement, reduction to ferrous iron and export of iron across the labyrinth. In contrast, *Hephl1* expression was predominantly concentrated to SynTII cells which lie adjacent to the fetal mesenchyme, positioning this ferroxidase at the final trophoblast layer before iron transfer into the fetal circulation (Fig. 2D).

Developmental trajectory analysis demonstrated coordinated maturation of these iron transport pathways between E9.5 and E14.5 (Fig. 2D). The images for each stage are shown in Suppl. Figure 1. Expression of the iron uptake receptor *Tfrc* and the iron exporter *Slc40a1* increased across multiple mature trophoblast populations, particularly SynTI, SynTII and S-TGCs, indicating progressive acquisition of iron transport capacity as the placental barrier differentiates and fetal iron demand increases. In contrast, regulatory genes associated with early trophoblast function and cellular adaptation, including *Hif1a*, *Aco1*, *Ireb2* and *Slc39a14*, generally declined with advancing gestation, consistent with trophoblast maturation and functional specialization of the exchange barrier. Thus, the observed expression trends reflect not only changing iron requirements during gestation but also differentiation of trophoblast cells towards specialized transport functions.

Ferroptosis-associated pathways were similarly enriched within the syncytiotrophoblast layers (Fig. 2D). Anti-ferroptotic genes including *Aifm2*, *Gpx4*, *Gclc*, *Gss*, *Slc7a11* and *Pcbp2* were highly expressed in SynTI and SynTII cells. Developmentally, *Aifm2* and *Gpx4* increased during trophoblast maturation, whereas *Gclc* and *Gss* declined in several lineages. The pro-ferroptotic mediator *Acsl4* increased in S-TGCs along the different stages of pregnancy but decreased in syncytiotrophoblast and glycogen cell populations, while *Pla2g6* showed increasing expression across several trophoblast lineages (Fig. 2D).

Collectively, these findings identify the syncytiotrophoblast layers as the principal cellular site integrating iron transport and ferroptosis-related pathways within the placenta. The spatial organization of iron uptake (*Tfrc*), intracellular transport (*Slc11a2*), iron export (*Slc40a1*) and fetal-facing oxidation (*Hephl1*) supports a continuous and largely unidirectional materno-fetal iron transport pathway. This concept is summarized in the working model shown in Fig. 2F, in which iron is acquired from maternal blood, trafficked through the syncytiotrophoblast layers and ultimately delivered to the fetal circulation through specialised fetal-facing trophoblast cells.


A
Placental cell clustering
UMAP_2
UMAP_1
Endothelial
Fetal mesenchyme
Decidua Stroma
Pericytes
Macro-phages
B-cells
NK-cells
Trophoblast clusters
Blood cells
T-cells
Erythrocytes
B
Trophoblast only clustering
SynTII
SynTII Precursor
S-TGC
LaTP
S-TGC Precursor
LaTP 2
SynTI Precursor
SynTI
JZP 1
JZP 2
SpT Precursor
Glycogen Cells
SpT
C
Placental cells
Fetal mesenchyme
Pericytes
Endothelial
Lymphatic endo.
Pro-angiogenic and lymphogenic lineages
Vascular endo.
Blood cells
NK-cells
T-cells
B-cells
Macrophages
Erythrocytes
Decidua / Stroma
Percent Expressed
Average Expression
Tfrc Lrp1 Scara5 Slc11a2 Slc39a8 Slc39a14 Slc40a1 Slc25a37 Slc25a28 Flvcr1 Flvcr2 Slc46a1 Slc48a1 Fth1 Cp Heph Hephl1 Hmox1 Hmox2 Steap3 Hamp Hfe Aco1 Ireb2 Dpp4 Acsl4 Hif1a Aifm2 Gpx4 Pla2g6 Gclc Gss Slc7a11 Sod1 Pcbp2
D
Trophoblast
LaTP
SynTII
SynTI
Glycogen Cells
SpT
S-TGC
Percent Expressed
Arrows:
Linear Trend direction over GA in mature cells
(E9.5, E10.5, E12.5, E14.5)
increasing
No significant trend
decreasing
Iron Endocytosis
Iron Transporters
Iron Storage
Oxido-reductases
Iron Regulators
anti-Ferroptosis
Pro-Ferroptosis
E
E14.5
Decidua Stroma
Trophoblast:
Labyrinth trophoblast progenitor (LaTP)
Sinusoidal trophoblast giant cells (S-TGC)
Syncytiotrophoblast layer (SynT)
SynTI/ SynTII
Spongiotrophoblasts (SpT)
Glycogen cells (GCs)
Fetal mesenchyme
Maternal blood
F
Endothelial cells
Fetal blood
Endosome
TFR1
2 Fe3+-Tf
STEAP3
DMT1
ZIP14
HFE
HEPC
Iron uptake in maternal gut
CP
HEPH
IRP1
FPN1
ACSL4
GPX4
Dpp4
FSP1
free Fe2+
Fenton reaction
Lipid peroxidation
Ferroptosis
Mitochondrion
HIF1α
HRG1
HCP1
FLVCR1
FLVCR2
Heme-Fe
Blood cells
S-TGC
FTH
SCARA5
Sinusoidal tropho-blast giant cell (S-TGC)
Fetal mesenchyme
SynT-II
Syncytiotrophoblast (SynT-I)
Maternal blood

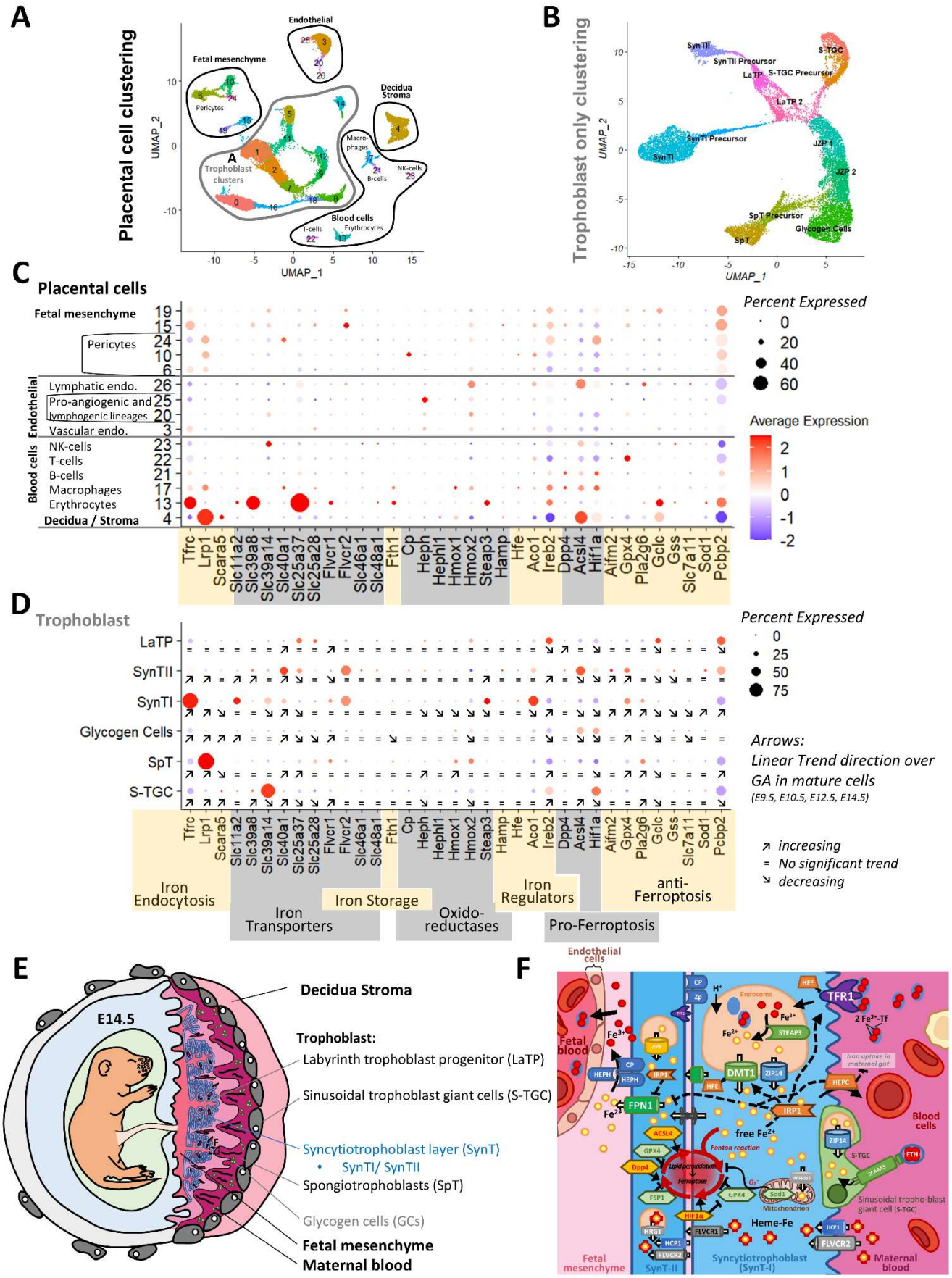


Figure 2: Placental iron handling is localized to the trophoblast barrier.

(A) UMAP of all placental nuclei at E14.5 showing major trophoblast, stromal, vascular and hematopoietic populations. (B) Trophoblast-only clustering identifying labyrinth trophoblast progenitors (LaTP), syncytiotrophoblast layer I (SynTI), syncytiotrophoblast layer II (SynTII), sinusoidal trophoblast giant cells (S-TGC), spongiotrophoblasts (SpT), glycogen cells and junctional zone progenitors (JzP1/JzP2). (C) Expression of iron homeostasis and ferroptosis-related genes across non-trophoblast placental populations. (D) Expression of the same gene set across

trophoblast populations. Dot size indicates the percentage of expressing cells and color indicates average normalized expression. Arrows indicate the direction of significant linear expression trends across gestation (E9.5, E10.5, E12.5 and E14.5) in mature trophoblast populations (↑ increasing; ↓ decreasing; = no significant trend). (E) Schematic of the E14.5 mouse placenta showing the spatial relationship between trophoblast lineages within the maternal-fetal exchange barrier. (F) Working model integrating snRNA-seq data with current knowledge of placental iron transport. Expression patterns support a sequential materno-fetal transfer pathway involving iron uptake, intracellular trafficking, export and oxidation across specialized trophoblast layers, while ferroptosis-regulatory pathways are concentrated within syncytiotrophoblast cells.
Dataset comprises >119,000 nuclei across four developmental stages [35]. Legend: LaTP, labyrinth trophoblast progenitor; SynTI, syncytiotrophoblast layer I; SynTII, syncytiotrophoblast layer II; S-TGC, sinusoidal trophoblast giant cell; SpT, spongiotrophoblast; UMAP, Uniform Manifold Approximation and Projection.

4.2 Pre-gestational maternal obesity induces metabolic remodeling while preserving maternal iron homeostasis

We next investigated whether pre-gestational maternal obesity disrupts iron handling during pregnancy. Female mice were fed either a chow or high-fat high-sugar (HFHS) diet for approximately nine weeks before conception and throughout pregnancy to establish a model of diet-induced pre-gestational obesity (Fig. 3A).

Maternal food consumption and energy intake changed across gestation but were broadly similar between dietary groups (Fig. 3F,G). In contrast, iron intake remained consistently lower in dams exposed to maternal obesity throughout pregnancy (Fig. 3H), reflecting the lower iron content of the obesogenic diet.

Despite reduced iron intake, maternal systemic iron homeostasis remained preserved at E18.5. Plasma iron concentration, transferrin saturation, total iron-binding capacity, circulating hepcidin concentrations and hematological indices were comparable between control dams and dams exposed to maternal obesity (Fig. 3I-O).

To further characterize the maternal phenotype, body composition and organ weights were assessed at E18.5 (Table 1). Maternal obesity dams exhibited a 10.2% reduction in post-hysterectomy body weight together with a marked 42.7% reduction in digestive tract mass, consistent with substantial physiological adaptation to pre-pregnancy obesogenic feeding (Table 1). Maternal obesity was also associated with pronounced organ remodeling, including hepatomegaly, with relative liver weight increased by 48.2%, and cardiac hypertrophy, with relative heart weight increased by 25.0% compared with controls (Table 1). In contrast, relative pancreas weight was reduced by 16.9% in maternal obesity dams (Table 1). Regional adipose tissue distribution was altered despite similar overall adiposity, with relative renal and gonadal fat mass reduced by 35.8% and 26.9%, respectively (Table 1). Relative brain weight was increased by 13.4%, largely reflecting the lower maternal body weight at term rather than changes in absolute brain mass (Table 1). Hepatomegaly, hepatic steatosis and metabolic dysfunction has been previously reported in HFHS-fed pregnant dams [5].

Collectively, these findings demonstrate that pre-pregnancy HFHS feeding induced a robust maternal obesity phenotype accompanied by substantial metabolic and anatomical changes, while systemic maternal iron homeostasis remained preserved despite reduced dietary iron intake. This model therefore enabled investigation of effects of maternal obesity on placental and fetal iron handling in the absence of overt maternal iron deficiency.

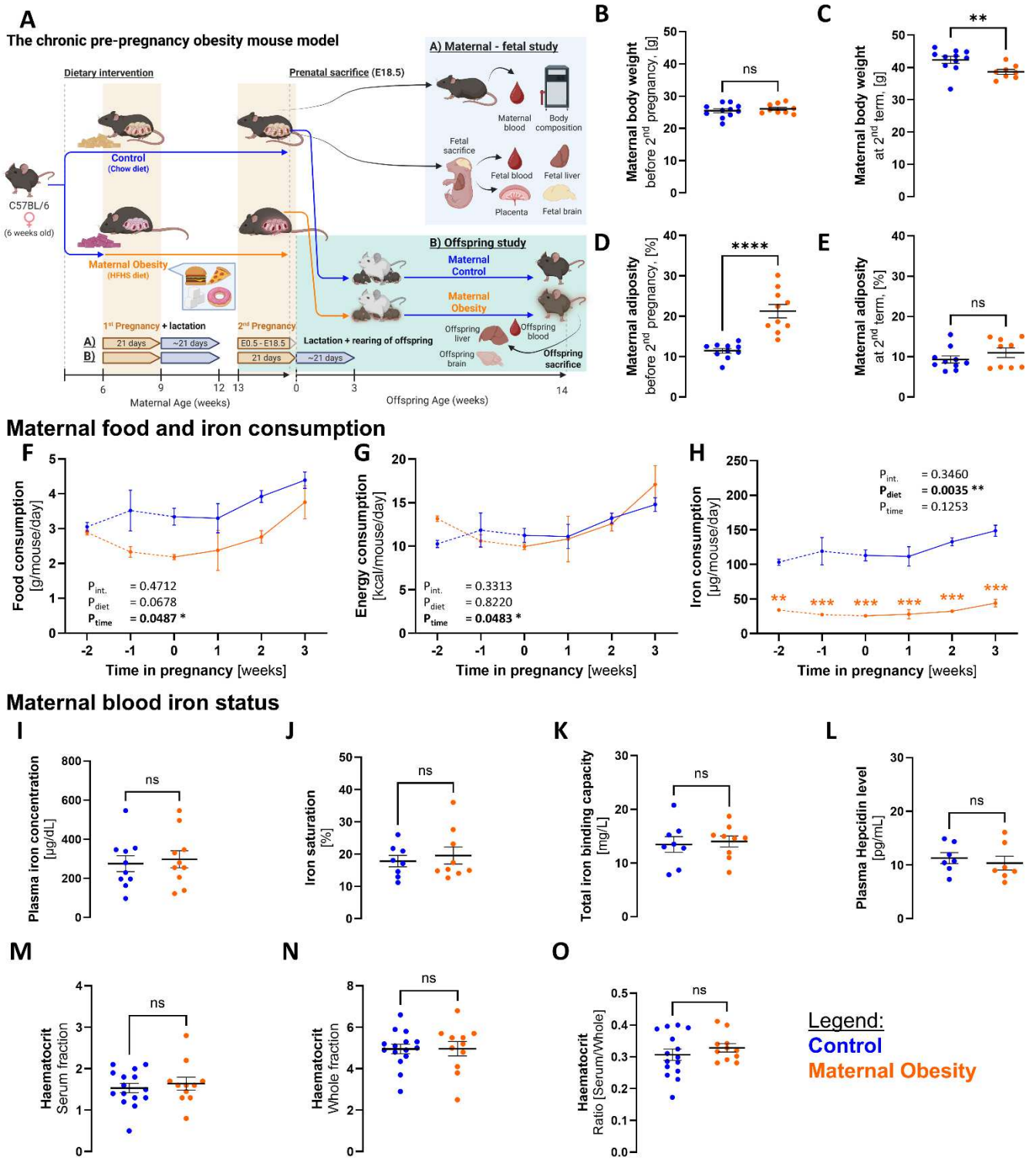


Figure 3: Maternal obesity remodels metabolism without maternal iron deficiency.

(A) Experimental design of the diet-induced pre-gestational obesity model. Females were maintained on chow or high-fat high-sugar (HFHS) diets before and throughout pregnancy. Maternal and fetal tissues were collected at E18.5, while a separate cohort was followed to 14 weeks of age for assessment of offspring outcomes. (B-E) Maternal body weight and adiposity before pregnancy and at E18.5. (F-H) Maternal food consumption, energy intake and iron intake during pregnancy. (I-O) Maternal circulating iron status and hematological indices at E18.5, including plasma iron concentration, transferrin saturation, total iron-binding capacity, plasma hepcidin concentration, and hematocrit measurements.

Data are mean ± SEM. Symbols represent individual dams. Blue symbols indicate chow-fed controls and orange symbols indicate dams exposed to maternal obesity. Longitudinal data (F-H) were analyzed using mixed-effects models with maternal diet and gestational age as fixed effects. Group comparisons (B-E, I-O) were performed using unpaired two-tailed tests as described in Methods. Statistical outcomes are shown within individual panels. *P < 0.05, **P < 0.01, ****P < 0.0001; ns, not significant. n = 8-15 dams per group.

Table 1: Maternal obesity alters body composition at late gestation.

Parameter	Control			Maternal obesity			T-test	Direction of change
	mean	± SEM	n	mean	± SEM	n		
Body weight post hysterectomy (BW) [g]	28.4	± 2.5	20	25.5	± 1.8	22	0.00010	*** ↘
Digestive tract [g]	3.79	± 0.19	10	2.17	± 0.16	6	0.00005	*** ↘
Brain (% BW)	1.49	± 0.03	20	1.69	± 0.03	22	0.00008	*** ↗
Heart (%BW)	0.52	± 0.02	20	0.65	± 0.02	22	0.00008	*** ↗
Liver (%BW)	7.43	± 0.12	20	11.01	± 0.26	22	<0.00001	*** ↗
Pancreas (%BW)	0.71	± 0.039	20	0.59	± 0.018	22	0.00547	** ↘
Renal fat (%BW)	0.53	± 0.0430	20	0.34	± 0.0239	22	0.00042	*** ↘
Gonadal fat (%BW)	1.19	± 0.11	20	0.87	± 0.06	22	0.01458	* ↘

Legend: Data are presented as mean ± SEM. Measurements were obtained from control dams (n = 20) and dams exposed to maternal obesity (n = 22) at E18.5 following hysterectomy. Organ weights are expressed relative to post-hysterectomy body weight unless otherwise indicated. Statistical significance was determined using unpaired two-tailed Student's t-tests.

4.3 Maternal obesity impairs feto-placental iron transport and remodels placental iron homeostasis and ferroptosis-associated pathways

Despite preserved maternal iron status (Fig. 3I-O), maternal obesity exposure impaired fetal iron acquisition at E18.5. Fetal serum iron concentrations were reduced in maternal obesity, with the largest effect observed in female fetuses, where circulating iron was 17% lower than in female controls (Fig. 4A). A similar pattern was observed for placental iron transport capacity, calculated as the feto-to-maternal iron ratio, which was reduced by 49% in female fetuses from obese dams (Fig. 4B). In contrast, litter size and sex distribution were unaffected by maternal diet (Fig. 4C).

Consistent with impaired maternal-fetal iron transfer, iron deposition within the placental labyrinth zone was reduced in maternal obesity pregnancies (Fig. 4D-F). Quantification of Prussian Blue staining demonstrated lower placental iron accumulation, accompanied by visibly fewer iron-positive deposits within the labyrinth zone of maternal obesity placentae compared with controls (Fig. 4E,F).

Maternal obesity also impaired placental growth. Placental weight was reduced by approximately 8% in both male and female maternal obesity pregnancies (Fig. 4G), whereas placental efficiency, assessed as the fetal-to-placental weight ratio, was unaffected (Fig. 4H). Together with the reduced iron deposition, these findings suggest that maternal obesity compromises placental development and iron storage while maintaining overall transfer efficiency relative to placental size.

To identify molecular mechanisms underlying these alterations, we re-analyzed placental labyrinth transcriptomic data from control and dams exposed to maternal obesity (Fig. 4I). The resulting expression profile revealed coordinated remodeling of genes involved in iron homeostasis and ferroptosis-associated pathways. Several antioxidant and anti-ferroptotic genes were downregulated in maternal obesity placentae, including *Sod1*, *Aifm2/Fsp1*, *Gss* and *Gpx4* (Fig. 4J-M). Expression of *Sod1* was reduced by 20-27%,

while *Aifm2/Fsp1* and *Gss* showed marked reductions in both sexes (Fig. 4J-L). These changes indicate diminished transcriptional capacity to counteract iron-dependent oxidative stress.

Alterations were also evident in genes regulating placental iron handling (Fig. 4N-T). Expression of the iron transporter *Slc46a1* was reduced, particularly in male placentae (Fig. 4N). In contrast, expression of *Pcbp2*, *Hamp*, *Ireb2*, *Hif1a*, *Slc25a37* and *Slc39a8* was increased following maternal obesity exposure (Fig. 4O-T). The strongest responses were observed for the iron-regulatory genes *Hamp*, *Ireb2* and *Hif1a*, which exhibited consistent increases across both sexes (Fig. 4P-R). However, several of these effects displayed sexual dimorphism, with greater responses for *Pcbp2*, *Ireb2*, *Hif1a* and *Acsl4* in females, and more pronounced changes in *Slc46a1* and *Slc25a37* in males (Fig. 4N-U). Notably, maternal obesity also increased expression of the pro-ferroptotic mediator *Acsl4* by 15-34%, particularly in female placentae (Fig. 4U). This latter finding further supports a shift towards a ferroptosis-prone placental phenotype.

Collectively, these findings demonstrate that maternal obesity reduces placental iron accumulation and fetal iron acquisition despite normal maternal iron status. These functional deficits are accompanied by extensive remodeling of placental iron-regulatory pathways and a transcriptional signature indicative of diminished anti-ferroptotic defenses and enhanced pro-ferroptotic signaling, suggesting increased susceptibility to ferroptosis in placental labyrinth of obese pregnant mice.

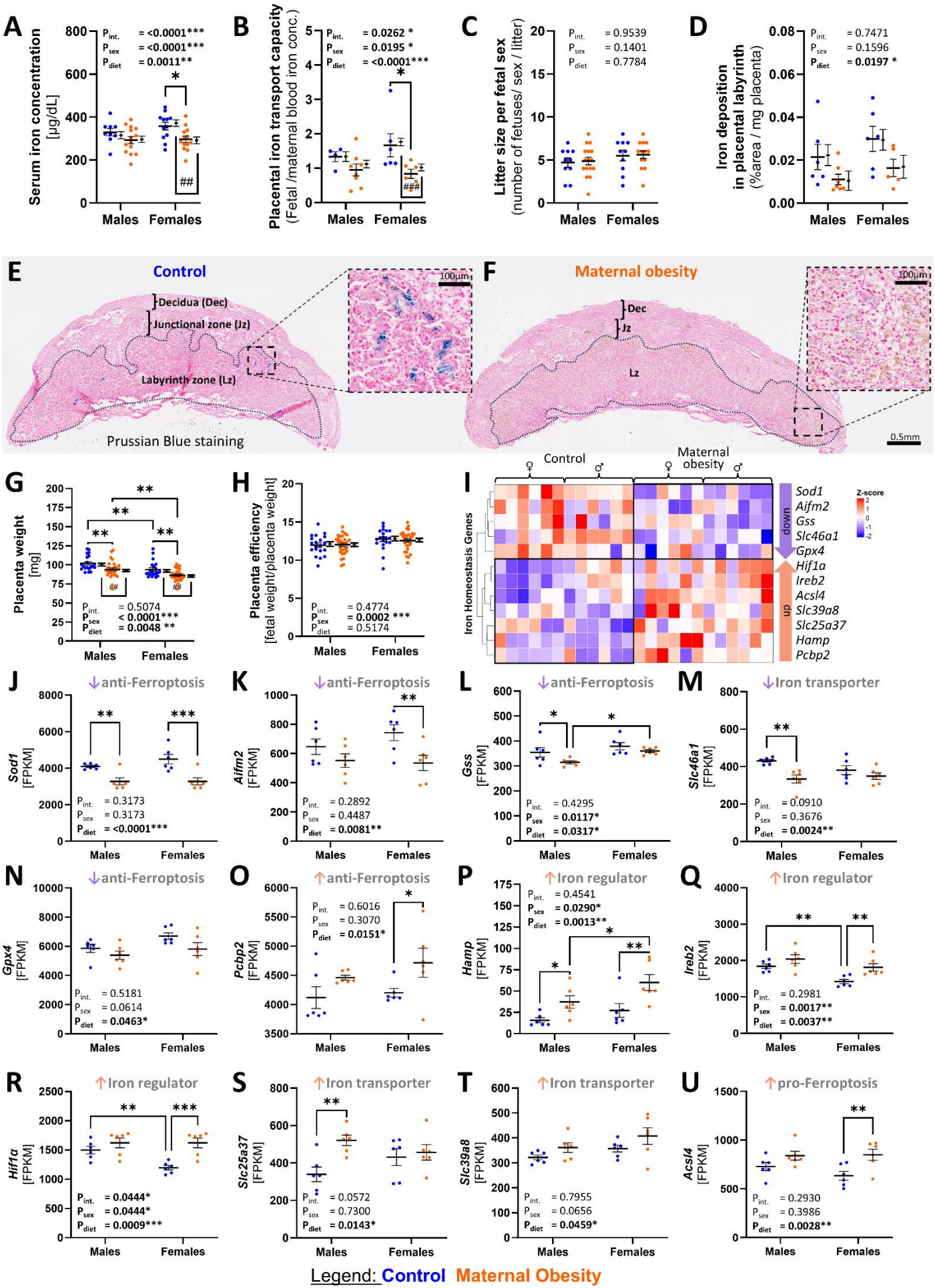

A
Serum iron concentration [µg/dL]
P int. = <0.0001***
P sex = <0.0001***
P diet = 0.0011**
Males Females
B
Placental iron transport capacity (Fetal /maternal blood iron conc.)
P int. = 0.0262 *
P sex = 0.0195 *
P diet = <0.0001***
C
Litter size per fetal sex (number of fetuses/ sex / litter)
P int. = 0.9539
P sex = 0.1401
P diet = 0.7784
D
Iron deposition in placental labyrinth (%area / mg placenta)
P int. = 0.7471
P sex = 0.1596
P diet = 0.0197 *
E
Control
Decidua (Dec)
Junctional zone (Jz)
Labyrinth zone (Lz)
Prussian Blue staining
100µm
F
Maternal obesity
Dec
Jz
Lz
0.5mm
G
Placenta weight [mg]
P int. = 0.5074
P sex = < 0.0001***
P diet = 0.0048 **
H
Placenta efficiency [fetal weight/placenta weight]
P int. = 0.4774
P sex = 0.0002 ***
P diet = 0.5174
I
Control
Maternal obesity
Iron Homeostasis Genes
down
up
Sod1
Aifm2
Gss
Slc46a1
Gpx4
Hif1a
Ireb2
Acsl4
Slc39a8
Slc25a37
Hamp
Pcbp2
Z-score
J
↓anti-Ferroptosis
Sod1 [FPKM]
P int. = 0.3173
P sex = 0.3173
P diet = <0.0001***
K
↓anti-Ferroptosis
Aifm2 [FPKM]
P int. = 0.2892
P sex = 0.4487
P diet = 0.0081**
L
↓anti-Ferroptosis
Gss [FPKM]
P int. = 0.4295
P sex = 0.0117*
P diet = 0.0317*
M
↓Iron transporter
Slc46a1 [FPKM]
P int. = 0.0910
P sex = 0.3676
P diet = 0.0024**
N
↓anti-Ferroptosis
Gpx4 [FPKM]
P int. = 0.5181
P sex = 0.0614
P diet = 0.0463*
O
↑anti-Ferroptosis
Pcbp2 [FPKM]
P int. = 0.6016
P sex = 0.3070
P diet = 0.0151*
P
↑Iron regulator
Hamp [FPKM]
P int. = 0.4541
P sex = 0.0290*
P diet = 0.0013**
Q
↑Iron regulator
Ireb2 [FPKM]
P int. = 0.2981
P sex = 0.0017**
P diet = 0.0037**
R
↑Iron regulator
Hif1α [FPKM]
P int. = 0.0444*
P sex = 0.0444*
P diet = 0.0009***
S
↑Iron transporter
Slc25a37 [FPKM]
P int. = 0.0572
P sex = 0.7300
P diet = 0.0143*
T
↑Iron transporter
Slc39a8 [FPKM]
P int. = 0.7955
P sex = 0.0656
P diet = 0.0459*
U
↑pro-Ferroptosis
Acsl4 [FPKM]
P int. = 0.2930
P sex = 0.3986
P diet = 0.0028**
Males Females
Legend: Control Maternal Obesity

Figure 4: Maternal obesity alters placental iron handling and ferroptosis pathways in the placental labyrinth zone.
(A-B) Fetal iron status at E18.5, including fetal serum iron concentration (A) and placental iron transport capacity calculated as the fetal-to-maternal iron ratio (B). (C) Litter size stratified by fetal sex. (D) Quantification of iron deposition within the placental labyrinth zone determined by Prussian Blue staining. (E-F) Representative placental sections from control (E) and maternal obesity (F) pregnancies showing reduced iron-positive staining within the labyrinth zone. Insets show higher-magnification views of the indicated regions. Dec, decidua; Jz, junctional zone; Lz, labyrinth zone. (G-H) Placental weight and placental efficiency (fetal:placental weight ratio). (I) Heatmap of selected iron homeostasis- and ferroptosis-related transcripts in placental labyrinth zone RNA-sequencing datasets grouped by maternal diet and fetal sex. Expression values are displayed as Z-scores. (J-M) Expression of anti-ferroptotic genes (*Sod1, Aifm2/Fsp1, Gss* and *Gpx4*). (N) Expression of the iron transporter *Slc46a1*. (O-T) Expression of iron regulatory and transport genes (*Pcbp2, Hamp, Ireb2, Hif1a, Slc25a37* and *Slc39a8*). (U) Expression of the pro-ferroptotic gene *Acsl4*.
Data are presented as mean ± SEM. Each symbol represents one fetus, placenta or biological replicate derived from an independent litter. Blue symbols indicate chow-fed controls and orange symbols indicate maternal obesity pregnancies. Statistical analyses for fetal and placental outcomes (A-H) were performed using linear mixed-effects models including maternal diet, fetal sex and their interaction as fixed effects, with litter included as a random effect. Transcript abundance data (J-U) were analyzed by two-way ANOVA with maternal diet and fetal sex as factors, followed by Fisher's least significant difference (LSD) post hoc test where appropriate. Interaction (*P*int), sex (*P*sex) and diet (*P*diet) effects are reported within individual panels; significant pairwise comparisons are indicated graphically. For transcriptomic analyses (I-U), $n = 6$ placentas per sex and dietary group. Scale bars: 0.5 mm (whole placental sections) and 100 μm (high-magnification insets).

4.4 Maternal obesity induces fetal growth restriction, reduces fetal iron accretion, and elicits tissue-specific molecular adaptations

Maternal obesity exposure impaired fetal growth at E18.5 (Fig. 5A-H). Fetal body weight was reduced by 7.5-8.5% in both sexes (Fig. 5A). This growth restriction was accompanied by a reduction in relative liver weight of 3.9-7.9% (Fig. 5B), whereas relative brain weight was increased by 2.1-7.1% (Fig. 5F), indicative of asymmetric growth restriction with relative brain sparing. Circulating fetal hepcidin concentrations were unchanged (Fig. 5E), suggesting that altered fetal iron status was not driven by systemic hepcidin signaling.

Consistent with reduced placental iron transport (Figs. 4A,B), fetal iron accretion was markedly impaired. Fetal liver iron concentration was reduced by 62-65%, resulting in a comparable reduction in total hepatic iron content of 72-76% (Fig. 5C,D). Maternal obesity also reduced fetal brain iron accretion, with brain iron concentration decreased by 23-27% and total brain iron content by 19-30% (Fig. 5G,H). These effects occurred similarly in both sexes and demonstrate that impaired placental iron transfer substantially limits iron accumulation in both major iron-storage and iron-dependent fetal organs.

To investigate molecular adaptations associated with fetal iron deficiency, expression of genes involved in iron homeostasis and ferroptosis was assessed in the fetal liver (Fig. 5I-M; Supplementary Table 2). Maternal obesity was associated with coordinated suppression of hepatic iron uptake and transport pathways. Expression of the iron uptake receptor *Tfrc* (TFR1) and the transporters *Slc11a2* (DMT1), *Slc39a8* (ZIP8) and *Slc40a1* (FPN1) were all reduced in maternal obesity exposed fetuses by -54%, -52%, -60% and -42% (Fig. 5I-J). Maternal diet accounted for a substantial proportion of the observed variation of expression between 19% - 35% (Supplementary Table 2), indicating coordinated suppression of multiple components of the hepatic iron acquisition machinery. Expression of the oxidoreductase *Heph* and the iron-sensing regulator *Aco1* (IRP1) were also reduced by -50% and -54% (Fig. 5K-L), with maternal diet explaining 19% and 27% of expression variance, respectively (Supplementary Table 2). Reduced expression

of the intracellular iron chaperone *Pcbp2* by -43% further suggests impaired intracellular iron trafficking within the fetal liver (Fig. 5M; Supplementary Table 2). Expression of *Gclc*, a key enzyme required for glutathione synthesis, represented the strongest transcriptional response of -73% to maternal obesity, with maternal diet accounting for approximately 41% of total expression variation. Maternal obesity also reduced expression of *Alox15* by -70% and *Ftmt* by -78%, for which maternal diet explained approximately 35% and 23% of expression variance, respectively (Supplementary Table 2). In contrast, expressions of *Gpx4*, *Gss*, *Aifm2/Fsp1* and *Slc7a11* were largely unaffected. The only prominent sex-dependent effect was observed for *Pla2g6*, where mRNA levels were reduced by -44% in females compared to males with fetal sex accounting for approximately 29% of expression variation (Fig. 5M; Supplementary Table 2). Together, these findings indicate that fetal hepatic adaptation to maternal obesity is driven predominantly by suppression of iron transport, iron regulation and selected antioxidant defense pathways.

The fetal brain exhibited a distinct transcriptional response (Fig. 5N-R; Supplementary Table 3). Similar to the liver, expression of *Tfrc* was increased by 28% in fetuses exposed to maternal obesity (Fig. 5N), with maternal diet explaining approximately 21% of total expression variance. The strongest dietary effects were observed for the iron transporters *Slc11a2* (-31%) and *Slc40a1* (-33%), for which maternal diet accounted for approximately 37% and 58% of expression variation, respectively (Fig. 5O; Supplementary Table 3). Expression of the oxidoreductase *Heph* was also reduced by -19%, with maternal diet explaining approximately 20% of expression variance (Fig. 5P; Supplementary Table 3). In contrast, expression of *Slc39a8*, *Hamp*, *Hfe* and *Ireb2* was largely unaffected (Fig. 5O,Q).

Unlike the fetal liver, several iron homeostasis genes in the fetal brain displayed pronounced sexual dimorphism. Fetal sex accounted for approximately 43% of the variation in *Slc11a2* expression, 34% of the variation in *Aco1* expression and 18% of the variation in *Slc39a14* expression (Fig. 5O,Q; Supplementary Table 3), indicating that sex was a major determinant of cerebral iron regulatory pathways with higher expression levels in female compared to male fetuses. Maternal obesity exerted relatively limited effects on ferroptosis-associated genes in the fetal brain (Fig. 5R). The principal dietary response was reduced expression of *Pla2g6* by -36%, for which maternal diet accounted for approximately 25% of expression variation (Supplementary Table 3). In contrast, antioxidant and intracellular iron-handling genes displayed strong sex-dependent regulation, including *Gss* (52%), *Pcbp2* (49%), *Gclc* (41%) and *Pla2g6* (31%) (Fig. 5R; Supplementary Table 3).

Collectively, maternal obesity induced asymmetric fetal growth restriction and substantially reduced iron accretion in both liver and brain. However, the molecular adaptations differed between tissues. The fetal liver responded predominantly through diet-dependent suppression of iron uptake, transport and antioxidant pathways, whereas the fetal brain exhibited a combination of reduced iron transport capacity and strong sex-dependent regulation of iron homeostasis and ferroptosis-associated networks. This divergence suggests distinct tissue-specific adaptations to reduced fetal iron availability during development.

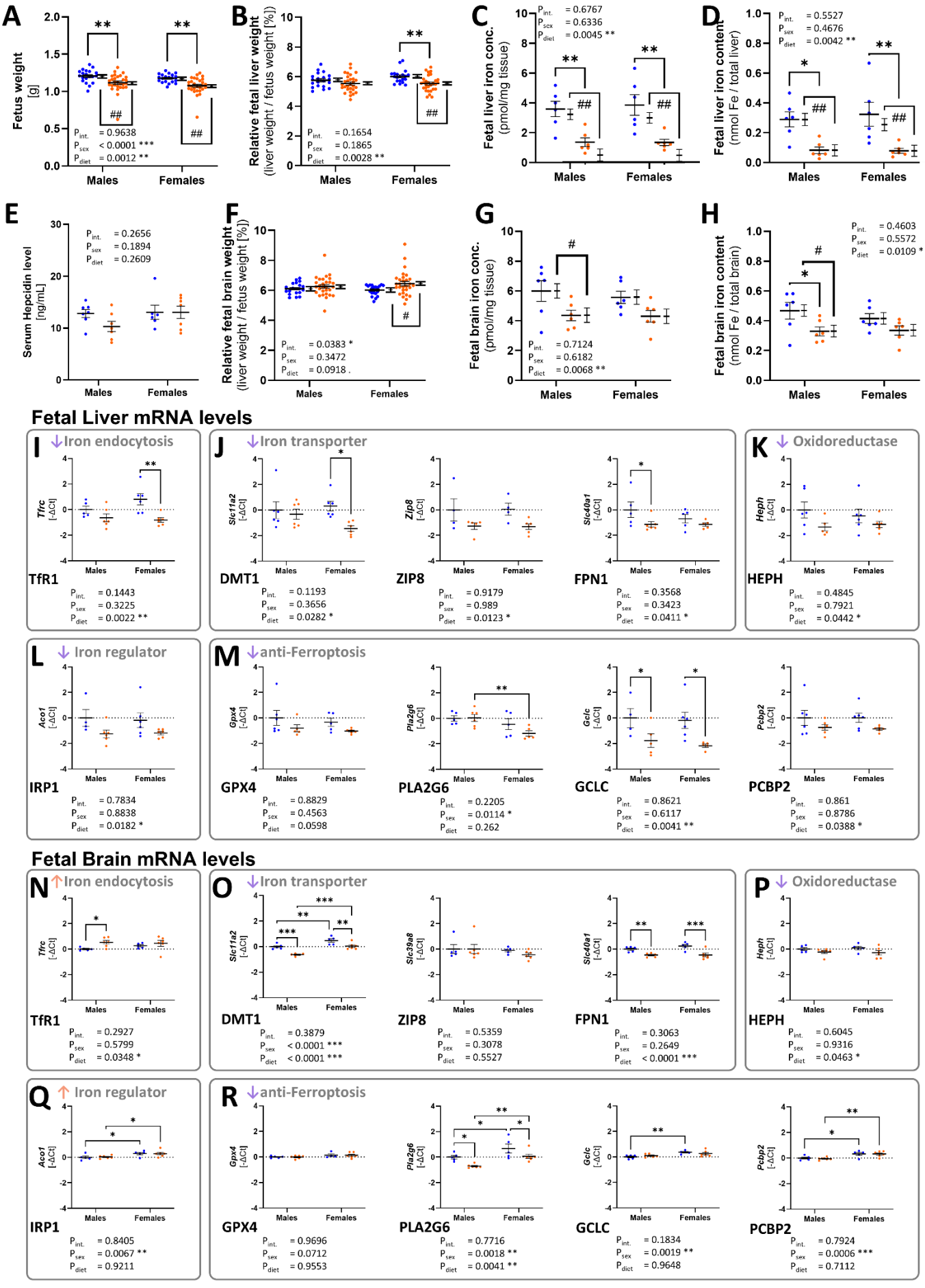

A
Fetus weight [g]
P int. = 0.9638
P sex < 0.0001 ***
P diet = 0.0012 **
Males
Females
B
Relative fetal liver weight (liver weight / fetus weight [%])
P int. = 0.1654
P sex = 0.1865
P diet = 0.0028 **
C
Fetal liver iron conc. (pmol/mg tissue)
P int. = 0.6767
P sex = 0.6336
P diet = 0.0045 **
D
Fetal liver iron content (nmol Fe / total liver)
P int. = 0.5527
P sex = 0.4676
P diet = 0.0042 **
E
Serum Hepcidin level [ng/mL]
P int. = 0.2656
P sex = 0.1894
P diet = 0.2609
F
Relative fetal brain weight (liver weight / fetus weight [%])
P int. = 0.0383 *
P sex = 0.3472
P diet = 0.0918 .
G
Fetal brain iron conc. (pmol/mg tissue)
P int. = 0.7124
P sex = 0.6182
P diet = 0.0068 **
H
Fetal brain iron content (nmol Fe / total brain)
P int. = 0.4603
P sex = 0.5572
P diet = 0.0109 *
Fetal Liver mRNA levels
I ↓Iron endocytosis
TfR1
P int. = 0.1443
P sex = 0.3225
P diet = 0.0022 **
J ↓Iron transporter
DMT1
P int. = 0.1193
P sex = 0.3656
P diet = 0.0282 *
ZIP8
P int. = 0.9179
P sex = 0.989
P diet = 0.0123 *
FPN1
P int. = 0.3568
P sex = 0.3423
P diet = 0.0411 *
K ↓ Oxidoreductase
HEPH
P int. = 0.4845
P sex = 0.7921
P diet = 0.0442 *
L ↓ Iron regulator
IRP1
P int. = 0.7834
P sex = 0.8838
P diet = 0.0182 *
M ↓anti-Ferroptosis
GPX4
P int. = 0.8829
P sex = 0.4563
P diet = 0.0598
PLA2G6
P int. = 0.2205
P sex = 0.0114 *
P diet = 0.262
GCLC
P int. = 0.8621
P sex = 0.6117
P diet = 0.0041 **
PCBP2
P int. = 0.861
P sex = 0.8786
P diet = 0.0388 *
Fetal Brain mRNA levels
N ↑Iron endocytosis
TfR1
P int. = 0.2927
P sex = 0.5799
P diet = 0.0348 *
O ↓Iron transporter
DMT1
P int. = 0.3879
P sex < 0.0001 ***
P diet < 0.0001 ***
ZIP8
P int. = 0.5359
P sex = 0.3078
P diet = 0.5527
FPN1
P int. = 0.3063
P sex = 0.2649
P diet < 0.0001 ***
P ↓ Oxidoreductase
HEPH
P int. = 0.6045
P sex = 0.9316
P diet = 0.0463 *
Q ↑ Iron regulator
IRP1
P int. = 0.8405
P sex = 0.0067 **
P diet = 0.9211
R ↓anti-Ferroptosis
GPX4
P int. = 0.9696
P sex = 0.0712
P diet = 0.9553
PLA2G6
P int. = 0.7716
P sex = 0.0018 **
P diet = 0.0041 **
GCLC
P int. = 0.1834
P sex = 0.0019 **
P diet = 0.9648
PCBP2
P int. = 0.7924
P sex = 0.0006 ***
P diet = 0.7112
Legend: Control Maternal Obesity

Figure 5: Maternal obesity induces asymmetric fetal growth and reduces tissue iron homeostasis in liver and brain.
(A-H) Fetal growth and tissue iron status at E18.5. Measurements include fetal body weight (A), relative liver weight (B), fetal liver iron concentration (C), total fetal liver iron content (D), circulating fetal hepcidin concentration (E), relative brain weight (F), fetal brain iron concentration (G) and total fetal brain iron content (H). (I-M) Fetal liver mRNA expression of genes involved in iron uptake, transport, regulation, oxidoreductase activity and ferroptosis-related pathways, including *Tfrc* (protein name = TFR1), *Slc11a2* (DMT1), *Slc39a8* (ZIP8), *Slc40a1* (FPN1), *Heph* (HEPH), *Aco1* (IRP1), *Gpx4* (GPX4), *Pla2g6* (PLA2G6), *Gclc* (GCLC) and *Pcbp2* (PCBP2). (N-R) Fetal brain mRNA expression of the corresponding iron homeostasis and ferroptosis-related genes.

Data are presented as mean ± SEM. Each symbol represents one fetus derived from an independent litter. Blue symbols indicate chow-fed controls and orange symbols indicate maternal obesity pregnancies. Gene expression was quantified by RT-qPCR and expressed relative to the control male group. Fetal growth and iron status outcomes (A-H) were analysed using linear mixed-effects models including maternal diet, fetal sex and their interaction as fixed effects, with litter size included as a covariate and dam identity as a random effect. Gene expression data (I-R) were analysed by two-way ANOVA with maternal diet and fetal sex as factors, followed by Fisher's least significant difference (LSD) post hoc test where appropriate. Interaction (*P*int), sex (*P*sex) and diet (*P*diet) effects are displayed within individual panels. Statistical annotations above individual comparisons denote significant post hoc differences identified by two-way ANOVA ($P < 0.05$, $\mathbf{P} < 0.01$, $\boldsymbol{P} < 0.001$). Symbols (#, ##) denote significant effects detected by the linear mixed-effects model for fetal outcome measures ($P < 0.05$ and $P < 0.01$, respectively). Sample sizes: A,B,F, n = 20-29 fetuses/sex/group; C,D,G,H, n = 6 fetuses/sex/group; E, n = 6-7 fetuses/sex/group; I-R, n = 5-6 fetuses/sex/group.

Suppl. Table 2: Effects of maternal obesity and fetal sex on fetal liver iron homeostasis and ferroptosis-related gene expression

Function	Gene (protein)	Sum of squares (Type III)	F-statistics (DFn, DFd)	% of total variation	P value	
Iron transporter	Slc39a14	0.1347	F (1, 18) = 0.1568	0.7105	$P_{sex*diet}$	0.6968
	(ZIP14)	0.09384	F (1, 18) = 0.1092	0.4948	P_{sex}	0.7449
		3.343	F (1, 18) = 3.890	17.63	P_{diet}	0.0641
Oxidoreductases	Cp	0.2203	F (1, 19) = 0.2269	1.014	$P_{sex*diet}$	0.6392
	(CP)	0.3706	F (1, 19) = 0.3818	1.705	P_{sex}	0.544
		2.878	F (1, 19) = 2.965	13.24	P_{diet}	0.1013
	Hephl1	164.8	F (1, 19) = 2.160	10.16	$P_{sex*diet}$	0.158
	(ZP)	0.8773	F (1, 19) = 0.01150	0.0541	P_{sex}	0.9157
		7.954	F (1, 19) = 0.1043	0.4905	P_{diet}	0.7503
	Hamp	1.218	F (1, 13) = 0.3261	2.342	$P_{sex*diet}$	0.5777
	(HEPC)	0.115	F (1, 13) = 0.03079	0.2212	P_{sex}	0.8634
		2.289	F (1, 13) = 0.6129	4.403	P_{diet}	0.4477
Iron regulators	Hfe	0.2563	F (1, 16) = 0.1496	0.7937	$P_{sex*diet}$	0.704
	(HFE)	1.318	F (1, 16) = 0.7694	4.082	P_{sex}	0.3934
		3.612	F (1, 16) = 2.109	11.19	P_{diet}	0.1658
	Ireb2	0.04148	F (1, 15) = 0.03835	0.2058	$P_{sex*diet}$	0.8474
	(IRP2)	0.2496	F (1, 15) = 0.2308	1.239	P_{sex}	0.6379
		3.437	F (1, 15) = 3.177	17.05	P_{diet}	0.0949
pro-Ferroptosis	Acsl4	0.2356	F (1, 18) = 0.3462	1.749	$P_{sex*diet}$	0.5636
	(ACSL4)	0.2999	F (1, 18) = 0.4407	2.227	P_{sex}	0.5152
		0.5958	F (1, 18) = 0.8754	4.424	P_{diet}	0.3619
	Alox15	4.293	F (1, 15) = 3.009	11.02	$P_{sex*diet}$	0.1033
	(ALOX15)	0.3514	F (1, 15) = 0.2462	0.9016	P_{sex}	0.6269
		13.57	F (1, 15) = 9.508	34.81	P_{diet}	0.0076 **
anti-Ferroptosis	Aifm2	0.6982	F (1, 14) = 0.5478	3.06	$P_{sex*diet}$	0.4715
	(FSP1)	0.1702	F (1, 14) = 0.1335	0.7459	P_{sex}	0.7202
		3.917	F (1, 14) = 3.074	17.17	P_{diet}	0.1014
	Ftmt	2.195	F (1, 15) = 0.4783	2.41	$P_{sex*diet}$	0.4998
	(FtMt)	1.302	F (1, 15) = 0.2836	1.429	P_{sex}	0.6022
		21.29	F (1, 15) = 4.639	23.37	P_{diet}	0.0479 *
	Gss	0.1291	F (1, 20) = 0.1374	0.5714	$P_{sex*diet}$	0.7148
	(GSS)	0.07935	F (1, 20) = 0.08446	0.3513	P_{sex}	0.7743
		3.588	F (1, 20) = 3.819	15.89	P_{diet}	0.0648
	Slc7a11	4.726	F (1, 20) = 0.5049	2.186	$P_{sex*diet}$	0.4856
	(xCT)	24.1	F (1, 20) = 2.575	11.15	P_{sex}	0.1243
		0.1751	F (1, 20) = 0.01871	0.08099	P_{diet}	0.8926

Legend: Two-way ANOVA (Type III sums of squares) was used to assess the effects of maternal diet, fetal sex, and diet × sex interaction on gene expression in fetal liver samples. For each factor, the table reports the Type III sum of squares, F statistic, percentage of total variance explained, and corresponding P value. Genes are grouped according to biological function, with encoded proteins indicated in parentheses. Significant effects are denoted as $P < 0.05$ (*) and $P < 0.01$ (**).

Genes: TFR1, transferrin receptor 1; DMT1, divalent metal transporter 1; ZIP8, Zrt- and Irt-like protein 8; ZIP14, Zrt- and Irt-like protein 14; FPN1, ferroportin 1; HEPH, hephaestin; IRP1, iron regulatory protein 1; ACSL4, acyl-CoA synthetase long-chain family member 4; ALOX15, arachidonate 15-lipoxygenase; FSP1, ferroptosis suppressor protein 1; FtMt, mitochondrial ferritin; GCLC, glutamate-cysteine ligase catalytic subunit; GPX4, glutathione peroxidase 4; GSS, glutathione synthetase; PCBP2, poly(rC)-binding protein 2; PLA2G6, phospholipase A2 group VI; xCT, cystine/glutamate antiporter.

Suppl. Table 3: Effects of maternal obesity and fetal sex on fetal brain iron homeostasis and ferroptosis-related gene expression

Function	Gene (protein)	Sum of squares (Type III)	F-statistics (DFn, DFd)	% of total variation	P value	
Iron transporter	Slc39a14	0.01807	F (1, 18) = 0.6009	2.218	$P_{sex*diet}$	0.4483
	(ZIP14)	0.1502	F (1, 18) = 4.996	18.45	P_{sex}	0.0383 *
		0.09396	F (1, 18) = 3.125	11.54	P_{diet}	0.094
Oxidoreductases	Cp	0.08068	F (1, 18) = 0.2773	1.48	$P_{sex*diet}$	0.6049
	(CP)	0.0006343	F (1, 18) = 0.002180	0.01164	P_{sex}	0.9633
		0.1323	F (1, 18) = 0.4548	2.428	P_{diet}	0.5086
	Hephl1	0.4684	F (1, 17) = 0.3066	1.608	$P_{sex*diet}$	0.587
	(ZP)	0.7797	F (1, 17) = 0.5103	2.676	P_{sex}	0.4847
		1.928	F (1, 17) = 1.262	6.62	P_{diet}	0.2768
	Hamp	5.574	F (1, 18) = 2.231	10.02	$P_{sex*diet}$	0.1526
	(HEPC)	1.142	F (1, 18) = 0.4569	2.052	P_{sex}	0.5077
		3.426	F (1, 18) = 1.371	6.158	P_{diet}	0.2569
Iron regulators	Hfe	0.1382	F (1, 18) = 1.562	7.502	$P_{sex*diet}$	0.2274
	(HFE)	0.09678	F (1, 18) = 1.093	5.252	P_{sex}	0.3095
		0.0339	F (1, 18) = 0.3830	1.84	P_{diet}	0.5438
	Ireb2	0.141	F (1, 18) = 1.590	6.688	$P_{sex*diet}$	0.2234
	(IRP2)	0.2126	F (1, 18) = 2.399	10.09	P_{sex}	0.1388
		0.1876	F (1, 18) = 2.116	8.898	P_{diet}	0.163
pro-Ferroptosis	Acsl4	0.3303	F (1, 18) = 2.287	9.219	$P_{sex*diet}$	0.1478
	(ACSL4)	0.03241	F (1, 18) = 0.2244	0.9045	P_{sex}	0.6414
		0.5991	F (1, 18) = 4.149	16.72	P_{diet}	0.0566
	Alox15	1.051	F (1, 18) = 1.674	7.664	$P_{sex*diet}$	0.2121
	(ALOX15)	0.7786	F (1, 18) = 1.240	5.676	P_{sex}	0.2802
		0.4021	F (1, 18) = 0.6403	2.931	P_{diet}	0.434
anti-Ferroptosis	Aifm2	0.7666	F (1, 18) = 1.979	8.573	$P_{sex*diet}$	0.1765
	(FSP1)	0.5582	F (1, 18) = 1.441	6.242	P_{sex}	0.2455
		0.7536	F (1, 18) = 1.945	8.427	P_{diet}	0.1801
	Ftmt	16.49	F (1, 18) = 2.450	11.58	$P_{sex*diet}$	0.1349
	(FtMt)	0.03042	F (1, 18) = 0.004521	0.02138	P_{sex}	0.9471
		4.402	F (1, 18) = 0.6542	3.093	P_{diet}	0.4292
	Gss	0.00001367	F (1, 18) = 0.0004307	0.001136	$P_{sex*diet}$	0.9837
	(GSS)	0.6253	F (1, 18) = 19.70	51.96	P_{sex}	0.0003 ***
		0.0008591	F (1, 18) = 0.02706	0.07139	P_{diet}	0.8712
	Slc7a11	0.05584	F (1, 18) = 0.2084	1.072	$P_{sex*diet}$	0.6535
	(xCT)	0.1485	F (1, 18) = 0.5542	2.852	P_{sex}	0.4662
		0.1935	F (1, 18) = 0.7220	3.716	P_{diet}	0.4067

Legend: Two-way ANOVA (Type III sums of squares) was used to assess the effects of maternal diet, fetal sex, and diet × sex interaction on gene expression in fetal brain samples. For each factor, the table reports the Type III sum of squares, F statistic, percentage of total variance explained, and corresponding P value. Genes are grouped according to biological function, with encoded

proteins indicated in parentheses. Significant effects are denoted as $P < 0.05$ (*) and $P < 0.001$ (***). The percentage of total variance represents the proportion of overall gene-expression variability explained by each factor in the model.

Gene names: as defined for Supplementary Table 2.

4.5 Recovery of hepatic but not cerebral iron homeostasis reveals persistent brain-specific programming of ferroptosis pathways

To determine whether the effects of maternal obesity on iron homeostasis persisted beyond fetal life, offspring from chow-fed and offspring from maternal obesity pregnancies were weaned onto a standard chow diet and examined at 14 weeks of age (Fig. 6A-H). Adult body weight was unaffected by maternal diet, but females remained 16-18% lighter than males irrespective of prenatal exposure (Fig. 6A; Table 2). Maternal obesity was associated with a modest increase in absolute brain weight of 4.3-4.8% and a reduction of 1.5-7.9% in relative liver weight, most evident in males (Fig. 6B,F; Table 2). Several organs displayed marked sexual dimorphism, with females exhibiting greater relative brain, spleen, adrenal and renal fat mass, whereas males had greater heart, liver and kidney weights (Table 2). Circulating iron concentrations were similar between groups (Fig. 6E), indicating normalization of systemic iron status despite prenatal exposure to maternal obesity.

Although circulating iron homeostasis recovered, tissue-specific differences persisted (Fig. 6C,D,G,H; Table 2). Liver iron concentration and total liver iron content were no longer affected by maternal diet (Fig. 6C,D), indicating recovery of hepatic iron stores. In contrast, the brain remained selectively vulnerable. Brain iron concentration was reduced by 14-15% in male and female offspring exposed to maternal obesity (Fig. 6G), while total brain iron content was reduced by 11-12% (Fig. 6H; Table 2). These findings demonstrate that impaired fetal brain iron accretion was not fully corrected after birth and persisted into adulthood despite restoration of systemic and hepatic iron homeostasis.

To assess molecular adaptations associated with these phenotypes, expression of iron homeostasis- and ferroptosis-related genes was examined in adult liver (Fig. 6I-M; Supplementary Table 4). In contrast to the extensive transcriptional changes observed in fetal liver, maternal obesity exerted little long-term effect on adult hepatic iron regulatory pathways. Expression of *Tfrc*, *Slc11a2*, *Aco1*, *Ireb2*, *Cp* and *Hfe* was unchanged (Fig. 6I-L). Instead, adult hepatic iron homeostasis was influenced predominantly by offspring sex. Female offspring exhibited higher expression of *Slc39a8* (+29%), *Slc40a1* (+43%), *Slc39a14* (+30%), *Heph* (+33%), and *Hamp* (+83%), whereas lower expression of *Gpx4* (-20%), *Pla2g6* (-32%) and *Gclc* (-27%) (Fig. 6J-L, Supplementary Table 4), indicating that sex rather than maternal diet had become the dominant determinant of hepatic iron homeostasis.

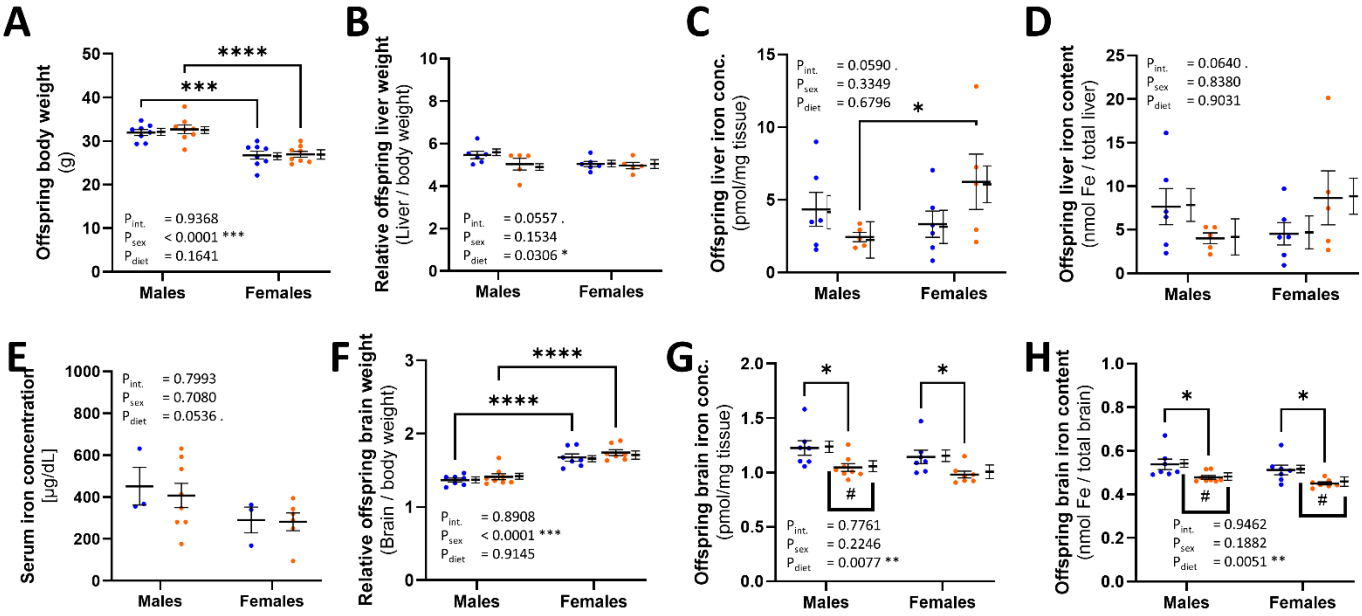
Long-term effects of maternal obesity in the liver were more evident within ferroptosis-associated pathways (Fig. 6M; Supplementary Table 4). Expression of *Gpx4* was increased by 23% following maternal obesity exposure and was 20% lower in female than male offspring. Diet, sex, and their interaction jointly accounted for approximately 40% of total expression variance,

with the dietary effect occurring primarily in males (Fig. 6M). Similarly, *Pla2g6* expression was higher in males and exhibited a significant diet-by-sex interaction, indicating sex-specific transcriptional responses to maternal obesity (Fig. 6M; Supplementary Table 4). In contrast, several ferroptosis-associated transcripts (*Alox15, Aifm2, Ftmt, Slc7a11* and *Hephl1*) were not detected in adult liver tissue. Collectively, these findings indicate that fetal alterations in hepatic iron homeostasis largely resolved by adulthood, whereas persistent sex-dependent changes in ferroptosis-associated pathways suggest sustained molecular programming of hepatic oxidative stress responses.

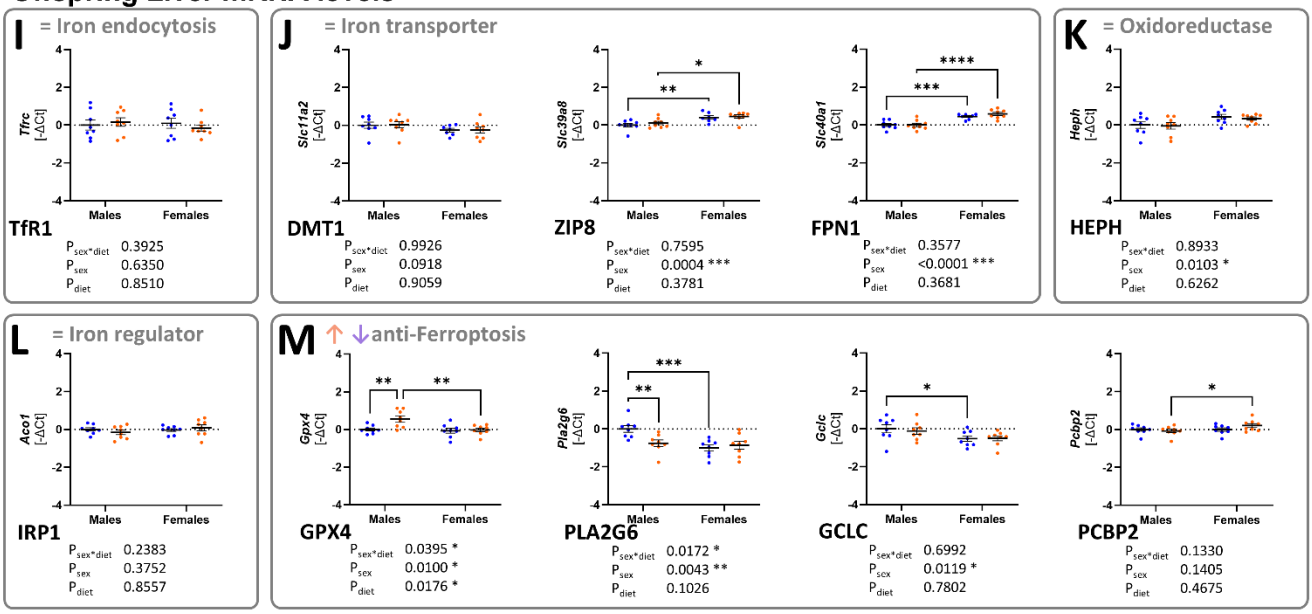
The adult brain displayed a markedly different pattern (Fig. 6N-R; Supplementary Table 5). Persistent reductions in brain iron concentration and content occurred despite largely preserved expression of canonical iron uptake genes such as *Tfrc* and *Slc11a2* (Fig. 6N,O). Instead, adult cerebral iron homeostasis was characterized by extensive sex-dependent regulation. Female offspring exhibited higher expression of *Slc39a8* by -47% and *Heph* by -42% than males (Fig. 6O,P), with sex accounting for approximately 25% and 19% of total expression variance, respectively (Supplementary Table 5). Furthermore, *Slc39a8*, *Slc39a14* and *Aco1* exhibited significant sex-dependent responses to maternal obesity, indicating persistent remodeling of cerebral iron regulatory pathways (Fig. 6O,Q).

The most pronounced long-term effects were observed among ferroptosis-related genes (Fig. 6R; Supplementary Table 5). Maternal obesity increased expression of *Gclc* (+74%), with maternal diet accounting for approximately 20% of total expression variation, suggesting persistent compensatory remodeling of glutathione synthesis pathways. Several ferroptosis-associated genes also displayed strong sex-dependent regulation. Expression of *Gpx4* and *Pla2g6* was with both -52% substantially lower in females than males, with offspring sex explaining approximately 43% and 41% of total variation, respectively (Supplementary Table 5). In contrast, *Pcbp2* expression was decreased (-40%) in females and strongly influenced by both sex and prenatal diet exposure (Fig. 6R), whereas *Ftmt* exhibited the largest interaction effect observed in the study (Supplementary Table 5). Together, these findings indicate persistent and sexually dimorphic remodeling of cerebral ferroptosis-related networks following prenatal exposure to maternal obesity.

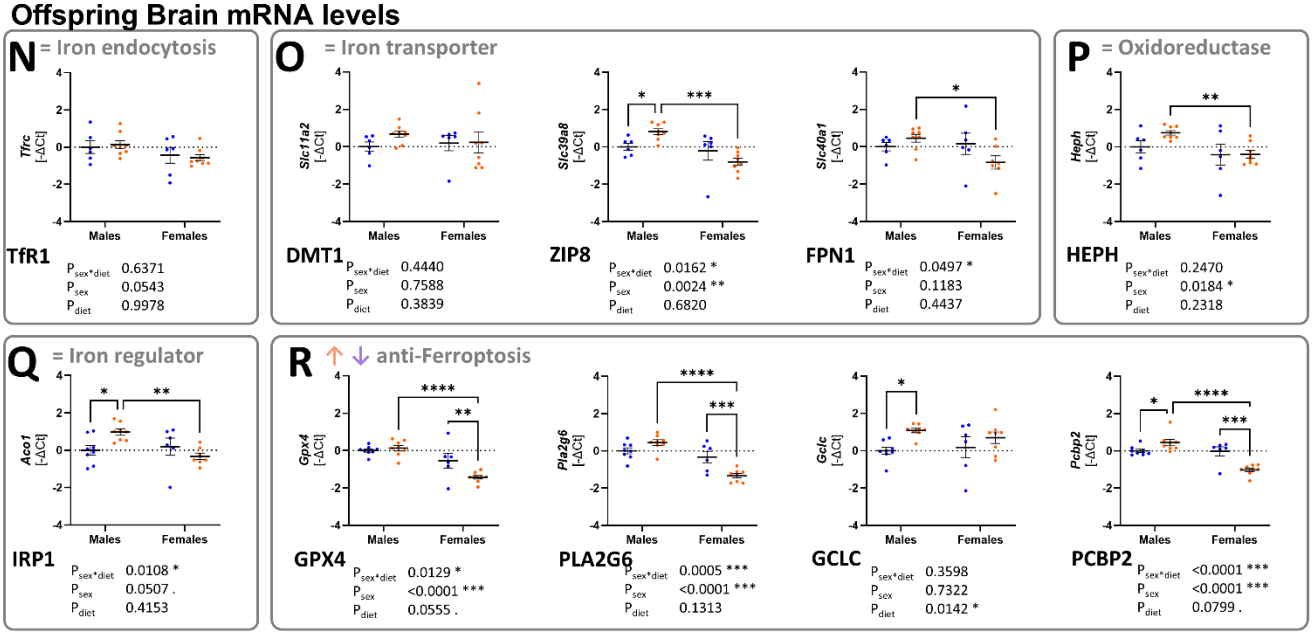
Overall, the consequences of maternal obesity persisted despite normalization of postnatal diet. While systemic iron status and hepatic iron stores recovered by adulthood, offspring exposed to maternal obesity exhibited persistent brain iron deficiency together with sustained alterations in cerebral iron homeostasis and ferroptosis-associated pathways. These data identify the brain as a particularly vulnerable target of developmental programming and support the concept that impaired placental iron transfer during gestation contributes to long-term alterations in offspring iron metabolism and redox regulation.



Offspring Liver mRNA levels



Offspring Brain mRNA levels



Legend: Control Maternal Obesity

Figure 6: Maternal obesity induces persistent brain iron deficiency and ferroptosis pathway remodeling in adult offspring
(A–H) Growth, tissue iron status and organ weight measurements in offspring at 14 weeks of age, including body weight (A), relative liver weight (B), liver iron concentration (C), total liver iron content (D), serum iron concentration (E), relative brain weight (F), brain iron concentration (G) and total brain iron content (H). (I-M) Adult liver mRNA expression of genes involved in iron uptake, transport, regulation, oxidoreductase activity and ferroptosis-related pathways, including *Tfrc* (TFR1), *Slc11a2* (DMT1), *Slc39a8* (ZIP8), *Slc40a1* (FPN1), *Heph* (HEPH), *Aco1* (IRP1), *Gpx4* (GPX4), *Pla2g6* (PLA2G6), *Gclc* (GCLC) and *Pcbp2* (PCBP2). (N-R) Adult brain mRNA expression of corresponding iron homeostasis and ferroptosis-related genes. Genes not detected or not assessed in adult liver and brain tissues are reported in Supplementary Tables 4 and 5.
Data are presented as mean ± SEM. Each symbol represents one offspring. Blue symbols indicate offspring born to chow-fed dams and orange symbols indicate offspring from maternal obesity pregnancies. Gene expression was quantified by RT-qPCR and expressed relative to the male control group. Adult physiological and tissue iron outcomes (A-H) were analysed using linear models including maternal diet, offspring sex and their interaction as fixed effects. Gene expression data (I-R) were analysed by two-way ANOVA with maternal diet and offspring sex as factors, followed by Fisher's least significant difference (LSD) post hoc test where appropriate. Interaction (*P*int), sex (*P*sex) and diet (*P*diet) effects are displayed within individual panels. Statistical annotations above pairwise comparisons denote significant post hoc differences identified by two-way ANOVA ($P < 0.05$, $P < 0.01$, $P < 0.001$, $P < 0.0001$). Symbols (#) indicate significant effects detected by the linear model for tissue iron measurements ($P < 0.05$). Sample sizes: A,B,F, n = 7-8 offspring/sex/group; C,D, n = 5-6 offspring/sex/group; E, n = 3-8 offspring/sex/group; G,H, n = 7-8 offspring/sex/group; I-R, n = 6-8 offspring/sex/group.

Table 2: Long-term effects of maternal obesity on offspring body composition, tissue iron status and organ weights at 14 weeks of age.

	Control				**Maternal obesity**				Linear modelling†		
	♂		♀		♂		♀				
	mean	± SEM	mean	± SEM	mean	± SEM	mean	± SEM	$P_{int.\ (sex * diet)}$	P_{sex}	P_{diet}
Offspring weight [g]	31.9	± 0.794	26.3	± 0.794	32.3	± 0.794	27.0	± 0.843	0.9204	<0.0001***	0.3803
Blood glucose fed state [mM]	11.1	± 0.658	10.4	± 0.658	8.8	± 0.620 *	11.1	± 0.658	0.0281 *	0.2173	0.1854
Liver iron conc. (pmol/mg tissue weight)	4.34	± 1.14	3.33	± 1.14	2.43	± 1.25	6.24	± 1.25	0.0590 .	0.3349	0.6796
Liver iron content (nmol/full liver)	7.66	± 1.88	4.53	± 1.88	4.01	± 2.06	8.66	± 2.06	0.0640 .	0.8380	0.9031
Brain iron conc. (pmol/mg tissue weight)	1.22	± 0.0510	1.14	± 0.0510	1.05	± 0.0477 *	0.98	± 0.0510 *	0.8686	0.1526	0.0026 **
Brain iron content (nmol/full brain)	0.538	± 0.0171	0.512	± 0.0171	0.478	± 0.0160 *	0.450	± 0.0171 *	0.9600	0.1235	0.0015 **
Brain weight [g]	0.440	± 0.0094	0.437	± 0.0094	0.459	± 0.0094	0.458	± 0.0099	0.9138	0.8442	0.0484 *
Brain (% body weight)	1.38	± 0.0420	1.67	± 0.0420	1.43	± 0.0420	1.72	± 0.0563	0.8908	<0.0001***	0.9145
Heart weight [g]	0.182	± 0.0064	0.127	± 0.0064	0.178	± 0.0064	0.130	± 0.0068	0.6090	<0.0001***	0.8481
Heart (% body weight)	0.569	± 0.0201	0.483	± 0.0201	0.554	± 0.0201	0.493	± 0.0269	0.5766	0.0016 **	0.7643
Liver weight [g]	1.75	± 0.0615	1.31	± 0.0615	1.56	± 0.0615 *	1.31	± 0.0653	0.1518	<0.0001***	0.1670
Liver (% body weight)	5.50	± 0.152	4.98	± 0.152	4.82	± 0.152 **	4.96	± 0.204	0.0557 .	0.1534	0.0306 *
Spleen weight [g]	0.0910	± 0.0061	0.0870	± 0.0061	0.1022	± 0.0061	0.0941	± 0.0065	0.7434	0.3449	0.1433
Spleen (% body weight)	0.284	± 0.0199	0.331	± 0.0199	0.317	± 0.0199	0.376	± 0.0266	0.7731	0.0221 *	0.1629
Combined Kidney weight [g]	0.363	± 0.0136	0.275	± 0.0136	0.415	± 0.0136 *	0.302	± 0.0144	0.3681	<0.0001***	0.0038 **
Kidneys (% body weight)	1.14	± 0.0360	1.04	± 0.0360	1.28	± 0.0360 **	1.15	± 0.0483	0.5772	0.0075 **	0.0008 ***
Muscle weight [g]	0.148	± 0.0079	0.147	± 0.0079	0.172	± 0.0079 *	0.148	± 0.0084	0.1604	0.1377	0.1102
Muscle (% body weight)	0.466	± 0.0309	0.561	± 0.0309	0.537	± 0.0309	0.550	± 0.0415	0.2356	0.0795 .	0.3990
Pancreas weight [g]	0.205	± 0.0147	0.157	± 0.0147	0.228	± 0.0147	0.183	± 0.0156	0.9103	0.0039 **	0.0959 .
Pancreas (% body weight)	0.647	± 0.0475	0.593	± 0.0475	0.705	± 0.0475	0.708	± 0.0637	0.5892	0.5591	0.1010
Combined Adrenal weight [mg]	6.03	± 0.566	7.85	± 0.566	6.74	± 0.566	8.09	± 0.600	0.6802	0.0094 **	0.4567
Adrenals (% body weight)	0.0189	± 0.0022	0.0301	± 0.0022	0.0212	± 0.0022	0.0327	± 0.0030	0.9294	<0.0001***	0.7399
Combined Retro fat weight [g]	0.1410	± 0.0204	0.0935	± 0.0204	0.1367	± 0.0204	0.1129	± 0.0217	0.5718	0.0919 .	0.6935
Retro fat (% body weight)	0.448	± 0.0649	0.351	± 0.0649	0.417	± 0.0649	0.355	± 0.0870	0.8040	0.2479	0.9417
Combined Renal fat weight [g]	0.0572	± 0.0165	0.1399	±0.0165	0.0693	± 0.0165	0.1687	± 0.0175	0.6234	<0.0001***	0.3030
Renal fats (% body weight)	0.181	± 0.0458	0.525	± 0.0458	0.210	± 0.0458	0.551	± 0.0615	0.9767	<0.0001***	0.6633
Combined Gonadal fat weight [g]	0.495	± 0.0618	0.461	± 0.0618	0.506	± 0.0618	0.455	± 0.0656	0.8930	0.5085	0.9486
Gonadal fats (% body weight)	1.56	± 0.173	1.74	± 0.173	1.55	± 0.173	1.42	± 0.232	0.4220	0.7987	0.4391
Digestive tract weight [g]	3.58	± 0.177	3.24	± 0.194	3.34	± 0.153	3.03	± 0.177	0.9181	0.0753 .	0.2169
Digestive tract (% body weight)	11.3	± 0.442	12.1	± 0.484	10.2	± 0.383 .	11.7	± 0.542	0.5102	0.0216 *	0.0490 *
Combined Testis weight [g]	0.218	± 0.0065			0.222	± 0.0065					0.6790
Testes (% body weight)	0.684	± 0.0168			0.687	± 0.0168					0.9073
Combined Ovary weight [g]			0.0177	±0.0013			0.0167	± 0.0014			0.5908
Ovaries (% body weight)			0.0678	± 0.0045			0.0699	± 0.0060			0.7789
Combined Mammary gland weight [g]			0.391	± 0.0451			0.446	± 0.0451			0.4004
Mammary glands (% body weight)			1.46	± 0.135			1.50	± 0.171			0.8905

Legend. Data are presented as estimated marginal means ± SE from linear models including maternal diet, offspring sex, and the diet × sex interaction. Organ weights are shown as absolute values and, where indicated, relative to body weight. P values for diet × sex interaction (P_{int}), offspring sex (P_{sex}), and maternal diet (P_{diet}) are reported. Significant effects are indicated as $P < 0.05$, $P < 0.01$ and $P < 0.001$.

Suppl. Table 4: Effects of maternal obesity and offspring sex on liver iron homeostasis and ferroptosis-related gene expression in adult offspring.

Function	Gene (protein)	Sum of squares (Type III)	F-statistics (DFn, DFd)	% of total variation	P value		
Iron transporter	Slc39a14	0.02674	F (1, 28) = 0.1443	0.4141	$P_{sex*diet}$	0.7069	
	(ZIP14)	1.163	F (1, 28) = 6.276	18.01	P_{sex}	0.0183	
		0.08000	F (1, 28) = 0.4318	1.239	P_{diet}	0.5165	
Oxidoreductases	Cp	0.04961	F (1, 28) = 0.5661	1.955	$P_{sex*diet}$	0.4581	
	(CP)	0.02850	F (1, 28) = 0.3252	1.123	P_{sex}	0.5730	
		0.005913	F (1, 28) = 0.06747	0.2330	P_{diet}	0.7970	
	Hamp	0.1093	F (1, 28) = 0.1424	0.3950	$P_{sex*diet}$	0.7088	
	(HEPC)	6.042	F (1, 28) = 7.873	21.84	P_{sex}	0.0090	**
		0.02231	F (1, 28) = 0.02907	0.08066	P_{diet}	0.8658	
Iron regulators	Hfe	0.1689	F (1, 28) = 3.049	8.907	$P_{sex*diet}$	0.0918	
	(HFE)	0.03315	F (1, 28) = 0.5984	1.748	P_{sex}	0.4457	
		0.1431	F (1, 28) = 2.583	7.546	P_{diet}	0.1192	
	Ireb2	0.1398	F (1, 28) = 2.052	6.827	$P_{sex*diet}$	0.1631	
	(IRP2)	<0.000001	F (1, 28) = 4.129e-012	<0.000001	P_{sex}	>0.9999	
		0.0006125	F (1, 28) = 0.008992	0.02991	P_{diet}	0.9251	
pro-Ferroptosis	Acsl4	0.0006125	F (1, 28) = 0.002233	0.006973	$P_{sex*diet}$	0.9626	
	(ACSL4)	0.9096	F (1, 28) = 3.316	10.35	P_{sex}	0.0793	
		0.1945	F (1, 28) = 0.7093	2.215	Pdiet	0.4068	
anti-Ferroptosis	Gss	0.1352	F (1, 28) = 0.3290	1.151	$P_{sex*diet}$	0.5708	
	(GSS)	0.02616	F (1, 28) = 0.06366	0.2228	P_{sex}	0.8026	
		0.07459	F (1, 28) = 0.1815	0.6352	P_{diet}	0.6733	

Legend: Two-way ANOVA (Type III sums of squares) was used to assess the effects of maternal diet, offspring sex, and diet × sex interaction on gene expression in adult liver samples. For each factor, the table reports the Type III sum of squares, F statistic, percentage of total variance explained, and corresponding P value. Genes are grouped according to biological function, with encoded proteins indicated in parentheses. Genes not detected in adult liver cDNA are indicated accordingly. Significant effects are denoted as $P < 0.05$ (), $P < 0.01$ (), $P < 0.001$ () and $P < 0.0001$ (****). **Genes:** ZIP14, zinc transporter 14; CP, ceruloplasmin; HEPC, hepcidin; HFE, homeostatic iron regulator; IRP2, iron regulatory protein 2; ACSL4, acyl-CoA synthetase long-chain family member 4; GSS, glutathione synthetase

Suppl. Table 5: Effects of maternal obesity and offspring sex on brain iron homeostasis and ferroptosis-related gene expression in adult offspring.

Function	Gene (protein)	Sum of squares (Type III)	F-statistics (DFn, DFd)	% of total variation	P value		
Iron transporter	Slc39a14	3.513	F (1, 23) = 4.292	13.76	$P_{sex*diet}$	0.0497	*
	(ZIP14)	2.155	F (1, 23) = 2.633	8.444	P_{sex}	0.1183	
		0.4972	F (1, 23) = 0.6075	1.948	P_{diet}	0.4437	
pro-Ferroptosis	Alox15	15.23	F (1, 23) = 1.208	4.881	$P_{sex*diet}$	0.2831	
	(ALOX15)	3.250	F (1, 23) = 0.2577	1.041	P_{sex}	0.6165	
		4.446	F (1, 23) = 0.3525	1.424	P_{diet}	0.5585	
anti-Ferroptosis	Ftmt	47.66	F (1, 26) = 44.47	<0.0001	$P_{sex*diet}$	<0.0001	****
	(FtMt)	17.14	F (1, 26) = 15.99	0.0005	P_{sex}	0.0005	***
		2.419	F (1, 26) = 2.257	0.1451	P_{diet}	0.1451	

Legend: Two-way ANOVA (Type III sums of squares) was used to assess the effects of maternal diet, offspring sex, and diet × sex interaction on gene expression in adult brain samples. For each factor, the table reports the Type III sum of squares, F statistic, percentage of total variance explained, and corresponding P value. Genes are grouped according to biological function, with encoded proteins indicated in parentheses. Significant effects are denoted as $P < 0.05$ (*),$P < 0.001$ (***) and $P < 0.0001$ (****). The percentage of total variance represents the proportion of gene-expression variability explained by each factor in the ANOVA model. **Gene names:** as defined for Supplementary Table 4.

5 Discussion

Maternal obesity is associated with placental dysfunction, abnormal fetal growth, and increased susceptibility to metabolic and neurodevelopmental disorders in offspring, yet the mechanisms linking maternal metabolic dysfunction with long-term developmental programming remain incompletely understood [1, 4, 5]. The present study identifies placental iron dysregulation as a potential mechanistic pathway linking maternal obesity to fetal iron deficiency, fetal growth restriction, and persistent offspring brain iron deficiency. Our findings support a model in which maternal obesity disrupts placental iron handling, thereby uncoupling maternal and fetal iron homeostasis, limiting fetal iron acquisition and producing persistent brain-specific alterations in iron homeostasis. Specifically, pre-existing maternal obesity uncoupled maternal and fetal iron homeostasis, producing fetal iron deficiency despite preserved maternal systemic iron status. This reduction in fetal iron availability occurred alongside reduced placental iron deposition, impaired estimated placental iron transport capacity, extensive remodeling of placental iron homeostasis pathways, and a transcriptional profile consistent with increased ferroptosis susceptibility. By complementing placental transcriptomic analyses with developmental single-nucleus RNA sequencing datasets, we further demonstrate that syncytiotrophoblast cells represent the principal cellular site coordinating iron transport and ferroptosis-related pathways within the placental exchange barrier. Importantly, while circulating and hepatic iron status largely recovered postnatally, offspring exposed to maternal obesity exhibited persistent cerebral iron deficiency and sustained alterations in brain ferroptosis-related networks. Together, these findings suggest that altered placental iron handling may contribute to the reduction in fetal iron availability observed in maternal obesity and thereby influence long-term offspring brain iron homeostasis.

A major finding of this study is that fetal iron deficiency developed despite apparently adequate maternal iron status. Although dams exposed to maternal obesity consumed less dietary iron throughout gestation, maternal circulating iron concentrations, transferrin saturation, hepcidin levels, and hematological indices remained unchanged at term. Because maternal iron status was preserved while fetal circulating and tissue iron stores were markedly reduced, the observed fetal iron deficiency is most parsimoniously explained by impaired placental iron transfer rather than inadequate maternal iron availability. Under normal physiological conditions, placental iron transfer is tightly regulated to prioritize delivery of iron to the developing fetus, even in situations where maternal iron supply fluctuates [7, 18]. The observation that fetal iron deficiency developed despite preserved maternal iron homeostasis therefore suggests a failure of this adaptive transport system. Our findings are consistent with clinical studies demonstrating reduced cord-blood ferritin concentrations and lower neonatal iron stores in infants born to mothers with obesity despite relatively normal maternal iron indices [14, 36–38]. Collectively, these observations support the emerging concept that maternal obesity uncouples maternal and fetal iron homeostasis and identify the placenta as a likely site at which this dissociation occurs.

Multiple lines of evidence support the existence of impaired placental iron transfer in obese pregnancy. Maternal obesity was associated with reduced placental iron deposition and lower fetal circulating iron concentrations, together with evidence of impaired

placental iron transport capacity. These changes occurred alongside reduced placental weight, indicating that disturbances in iron handling were associated with broader alterations in placental development and function. At the molecular level, maternal obesity induced coordinated remodeling of placental iron-regulatory pathways, including increased expression of *Hamp*, *Ireb2*, *Hif1a*, *Slc25a37*, and *Slc39a8* and reduced expression of *Slc46a1*. Although the functional significance of individual transcriptional changes requires further investigation, the overall pattern suggests activation of stress-responsive mechanisms attempting to maintain intracellular iron homeostasis. Increased placental *Hamp* expression may limit ferroportin-mediated iron export, whereas elevated *Ireb2* and *Hif1a* expression may reflect compensatory responses to altered cellular iron availability, oxidative stress, or metabolic adaptation [7, 9]. Importantly, several responses exhibited fetal sex-dependence, suggesting that male and female placentae may utilize distinct adaptive mechanisms when challenged by maternal obesity. Taken together, reduced placental iron deposition, reduced feto-maternal iron ratio, altered expression of iron-regulatory genes, and diminished fetal iron stores indicate functional impairment of placental iron transfer, regardless of fetal sex.

To our knowledge, this is the first study to systematically integrate developmental single-nucleus RNA sequencing data with placental iron homeostasis analyses to demonstrate that syncytiotrophoblast cells constitute the principal cellular hub coordinating both iron transport and ferroptosis-associated pathways within the placental exchange barrier. While previous studies have identified individual transport proteins involved in placental iron transfer, the cellular architecture coordinating these pathways within the placental barrier has remained incompletely resolved [7, 9, 10]. Our analyses demonstrate that syncytiotrophoblast populations express the highest levels of genes involved in iron uptake, intracellular transport, storage, and export, including *Tfrc*, *Slc11a2*, *Slc40a1*, *Slc39a8*, *Slc48a1*, and *Slc25a37*. Furthermore, developmental analyses reveal progressive maturation of these pathways during gestation, consistent with increasing fetal iron requirements. Collectively, these observations identify syncytiotrophoblast cells as the principal cellular hub coordinating maternal iron acquisition, intracellular iron trafficking, fetal iron delivery and ferroptosis-associated pathways within the placental exchange barrier. Consequently, obesity-induced dysfunction within this trophoblast population may have disproportionate effects on fetal nutrient availability.

Our findings also implicate ferroptosis-associated pathways in obesity-induced placental dysfunction. Ferroptosis represents an iron-dependent form of regulated cell death driven by lipid peroxidation and failure of antioxidant defense systems [27, 39]. Growing evidence implicates ferroptosis in placental disorders including fetal growth restriction, preeclampsia, gestational diabetes, and maternal obesity [24–26]. In the present study, maternal obesity increased expression of the pro-ferroptotic mediator *Acsl4* while simultaneously reducing expression of several genes involved in antioxidant defence and ferroptosis suppression, including *Gpx4*, *Aifm2/Fsp1*, *Gss*, and *Sod1*. Importantly, developmental single-cell analyses demonstrated that many of these pathways are enriched within syncytiotrophoblast populations, positioning these cells at the intersection of iron transport and redox regulation. Iron homeostasis and ferroptosis are intrinsically linked biological processes, and disturbances in cellular iron trafficking can promote oxidative damage, lipid peroxidation, and ferroptosis susceptibility [27, 39]. The concurrent increase in *Acsl4* and reduction in *Gpx4*,

Aifm2/Fsp1, *Gss*, and *Sod1* indicate a transcriptional shift toward increased ferroptosis susceptibility within the placenta. Nevertheless, because the present study assessed transcriptional signatures rather than direct markers of ferroptotic activity, our findings should be interpreted as evidence of increased ferroptosis susceptibility rather than definitive evidence of ferroptotic cell death. Future studies assessing lipid peroxidation products, glutathione depletion, mitochondrial morphology, and ferroptosis-specific biomarkers will be important for establishing causality.

Impaired placental iron transfer was associated with substantial consequences for fetal development. Maternal obesity induced asymmetric fetal growth restriction accompanied by markedly reduced liver and brain iron accretion. These findings align with previous reports demonstrating that placental dysfunction associated with maternal obesity can alter nutrient partitioning and fetal growth trajectories [3–5]. They further align with the established role of placental iron transport in supporting fetal growth, organogenesis, mitochondrial function, and the accumulation of neonatal iron reserves [8, 11]. Despite broadly similar reductions in tissue iron accumulation, the fetal liver and brain exhibited distinct molecular adaptations. The fetal liver responded predominantly through diet-dependent suppression of pathways involved in iron uptake, transport, intracellular trafficking, and antioxidant defense. In contrast, the fetal brain displayed comparatively fewer diet-dependent transcriptional responses but pronounced sex-dependent regulation of iron homeostasis and ferroptosis-associated pathways. These findings suggest that developmental responses to reduced iron availability are highly tissue-specific and that male and female fetuses may engage distinct molecular strategies to adapt to nutrient restriction.

Although fetal iron deficiency affected multiple organs, the persistence of brain iron deficiency despite normalization of circulating and hepatic iron status identifies the developing brain as an exceptionally vulnerable target of maternal obesity-induced placental iron insufficiency. Another important finding of the present study was that reductions in fetal brain iron accretion persisted into adulthood despite complete recovery of systemic iron status and hepatic iron stores, providing evidence that placental iron dysregulation during pregnancy exerts lasting effects on offspring iron homeostasis. These observations suggest that impaired iron delivery during development cannot be fully compensated for after birth, even when nutritional iron supply is restored. Such vulnerability is biologically plausible because the developing brain has exceptionally high iron requirements during critical periods of neurogenesis, synaptogenesis, mitochondrial maturation, myelination, and neurotransmitter production [40–42]. Experimental models have repeatedly demonstrated that iron deficiency during early development induces long-lasting alterations in hippocampal structure and function, energy metabolism, learning, memory, and behaviour, many of which persist despite subsequent iron repletion [11, 43–45]. Consequently, the persistent reduction in adult brain iron observed in the present study likely represents more than a residual biochemical phenotype and instead may reflect incomplete recovery of developmental processes disrupted during fetal life.

The pattern observed across maternal, placental, fetal, and adult tissues supports a sequential biological model. Maternal obesity preserved maternal systemic iron status but reduced placental iron deposition and estimated placental iron transport capacity, leading

to reduced fetal circulating iron concentrations and diminished iron accretion in the fetal liver and brain [6, 21] . While hepatic iron stores recovered postnatally [46], brain iron deficiency persisted into adulthood [23, 47] . This progression is consistent with a model in which placental iron dysregulation precedes fetal and lifelong alterations in iron homeostasis and identifies impaired placental iron transport as a candidate driver of obesity-associated developmental programming [36].

The persistence of cerebral iron deficiency is of particular interest in the context of maternal obesity-associated neurodevelopmental risk. Iron serves essential roles in dopamine, serotonin, and glutamate signaling, mitochondrial respiration, and myelin formation, all of which are critical for normal cognitive and behavioral function [41, 42]. Accordingly, impaired placental iron transfer has been proposed as a potential contributor to neurodevelopmental abnormalities associated with maternal obesity [48, 49]. Although behavioral outcomes were not evaluated in the present study, the persistence of brain iron deficiency together with sustained alterations in iron-regulatory pathways suggests that placental iron dysregulation may contribute to long-term neurodevelopmental programming associated with maternal obesity. Together, these findings support the existence of a placenta-brain iron axis whereby disturbances in placental iron handling during gestation exert disproportionate and persistent effects on cerebral iron homeostasis.

Persistent alterations in ferroptosis-associated pathways within the adult brain further support the existence of long-lasting developmental remodeling. Maternal obesity increased cerebral *Gclc* expression and influenced the expression of several genes involved in antioxidant defense and intracellular iron handling, including *Ftmt*, *Pcbp2*, *Gpx4*, and *Pla2g6*. Many of these effects displayed significant interactions between maternal diet and offspring sex, indicating sexually dimorphic responses to altered fetal iron supply. Although the functional implications of these transcriptional changes remain uncertain, their persistence into adulthood alongside sustained reductions in brain iron content suggests durable remodeling of pathways involved in redox homeostasis and cellular resilience.

Several limitations should be acknowledged. First, placental iron transport capacity was inferred from the fetal-to-maternal circulating iron ratio rather than measured directly using isotope- or tracer-based approaches. Second, ferroptosis was inferred from transcriptomic signatures rather than assessed directly using biochemical, ultrastructural, or histological endpoints. Third, analyses were restricted to late gestation and adulthood, precluding evaluation of postnatal trajectories of iron homeostasis and developmental adaptation. Finally, neurobehavioral outcomes were not assessed, preventing direct evaluation of the functional consequences of persistent cerebral iron deficiency. Future studies incorporating direct measurements of placental iron transfer, ferroptosis-specific endpoints, longitudinal developmental analyses, and neurobehavioral assessments will be important for determining causality and identifying windows for therapeutic intervention.

In conclusion, the present study identifies placental iron dysregulation as a previously underappreciated mechanism linking maternal obesity with impaired fetal development and long-term offspring programming. Pre-gestational maternal obesity uncoupled maternal and fetal iron homeostasis, producing fetal iron deficiency despite preserved maternal systemic iron status. These alterations were associated with reduced placental iron deposition, diminished placental iron transport capacity, and coordinated

remodeling of iron homeostasis and ferroptosis-associated pathways within syncytiotrophoblast cells, the principal site of materno-fetal iron transfer. Impaired placental iron handling was accompanied by fetal growth restriction and markedly reduced fetal liver and brain iron accretion. Importantly, whereas systemic and hepatic iron homeostasis recovered postnatally, cerebral iron deficiency persisted into adulthood together with sustained alterations in ferroptosis-related gene networks. Collectively, our data support a model in which maternal obesity is associated with impaired placental iron handling and reduced fetal iron availability despite preserved maternal iron status. The persistence of brain iron deficiency into adulthood further indicates that placental iron transport may be an important determinant of long-term offspring iron homeostasis and contribute to obesity-associated neurodevelopmental programming.

6 Statements and Declarations

6.1 Funding

This work was supported by funding awarded to ANS-P from the Medical Research Council (MR/R022690/1/RG93186) and Lister Institute of Preventative Medicine (RG39692). JZ was supported by an SNSF Postdoc.Mobility fellowship (P500PB_206896). AAC was supported by CONICYT PFCHA/DOCTORADO NACIONAL/2019-21190352. Fondecyt 1220421 (BJK) and 1201283 (EAH). This work was also supported by the MRC MDU Mouse Biochemistry Laboratory (Core Biochemical Assay Laboratory, Cambridge) (MC_UU_00014/5).

6.2 Competing Interests

The authors have no relevant financial or non-financial interests to disclose.

6.3 Author contributions

J.Z. and A.N.S.-P. conceived and designed the study. S.C.L. and E.G. performed the mouse experiments. J.Z. conducted the single-nucleus RNA-sequencing analyses, histological studies, molecular analyses, and data interpretation. A.A.C. prepared samples for RNA sequencing of mouse placental tissue. M.V. quantified mRNA levels in fetal liver samples. I.B. isolated RNA and generated cDNA for qPCR analyses in fetal brain samples. J.Z. and A.N.S.-P. wrote the manuscript. All authors reviewed the final version and approved the manuscript for publication.

6.4 Data Availability

The experimental data that support the findings of this study are available in Zenodo (https://doi.org/10.5281/zenodo.21700146). Publicly available datasets analyzed during the current study are available through GEO under accessions GSE262011 and GSE152248.

6.5 Ethics approval and consent to participate

All animal procedures were performed under the UK Home Office Animals (Scientific Procedures) Act 1986 and approved by the University of Cambridge Animal Welfare and Ethical Review Board. Archival samples from previously published studies (Candia et al., 2024) were reused in accordance with the principles of the UK Home Office 3Rs to maximize scientific output and minimize animal use.

6.6 Consent to publish

Not applicable. This manuscript does not contain identifiable human participant data.

6.7 Clinical trial number

Clinical trial number: not applicable.

6.8 Acknowledgements

We thank Emma J. Siragher for her assistance with single-nucleus RNA sequencing (snRNA-seq) data analysis using Seurat in RStudio. We are also grateful to the staff of the Combined Animal Facility at the University of Cambridge, UK, for their excellent support with mouse husbandry and animal care.

7 References

1. Fowden AL, Camm EJ, Sferruzzi-Perri AN (2020) Effects of Maternal Obesity On Placental Phenotype. Curr Vasc Pharmacol 19:113–131. https://doi.org/10.2174/1570161118666200513115316

2. Jeve YB, Konje JC, Doshani A (2015) Placental dysfunction in obese women and antenatal surveillance strategies. Best Pract Res Clin Obstet Gynaecol 29:350–364. https://doi.org/10.1016/j.bpobgyn.2014.09.007

3. Sferruzzi-Perri AN, Vaughan OR, Haro M, et al (2013) An obesogenic diet during mouse pregnancy modifies maternal nutrient partitioning and the fetal growth trajectory. FASEB Journal 27:3928–3937. https://doi.org/10.1096/fj.13-234823

4. Napso T, Lean SC, Lu M, et al (2022) Diet-induced maternal obesity impacts feto-placental growth and induces sex-specific alterations in placental morphology, mitochondrial bioenergetics, dynamics, lipid metabolism and oxidative stress in mice. Acta Physiol (Oxf) 234:e13795. https://doi.org/10.1111/apha.13795

5. Candia AA, Lean SC, Zhang CXW, et al (2024) Obesogenic Diet in Mice Leads to Inflammation and Oxidative Stress in the Mother in Association with Sex-Specific Changes in Fetal Development, Inflammatory Markers and Placental Transcriptome. Antioxidants 13:411. https://doi.org/10.3390/ANTIOX13040411/S1

6. Zaugg J, Lopez-Tello J, Musial B, et al (2024) Obesogenic diet in pregnancy disrupts placental iron handling and ferroptosis and stress signalling in association with fetal growth alterations. Cellular and Molecular Life Sciences 2024 81:1 81:1–21. https://doi.org/10.1007/S00018-024-05192-5

7. Sangkhae V, Nemeth E (2018) Placental iron transport: The mechanism and regulatory circuits. Free Radic Biol Med 1–8. https://doi.org/10.1016/j.freeradbiomed.2018.07.001

8. McDonald EA, Gundogan F, Olveda RM, et al (2020) Iron transport across the human placenta is regulated by hepcidin. Pediatr Res 0–1. https://doi.org/10.1038/s41390-020-01201-y

9. Cao C, Fleming MD (2021) Localization and Kinetics of the Transferrin-Dependent Iron Transport Machinery in the Mouse Placenta. Curr Dev Nutr 5:nzab025. https://doi.org/10.1093/CDN/NZAB025

10. Santhakumar S, Edison ES (2023) Molecular insights into placental iron transfer mechanisms and maternofetal regulation. Archives of Gynecology and Obstetrics 2023 309:1 309:63–77. https://doi.org/10.1007/S00404-023-07032-6

11. Gundacker A, Glat M, Wais JP, et al (2023) Early-life iron deficiency persistently disrupts affective behaviour in mice. Taylor & Francis

12. Sangkhae V, Fisher AL, Chua KJ, et al (2020) Maternal hepcidin determines embryo iron homeostasis in mice. Blood 136:2206–2216. https://doi.org/10.1182/BLOOD.2020005745

13. Katsi V, Alifragki A, Fragkiadakis K, et al (2025) The Emerging Roles of Ferroptosis and NETosis in Pregnancy Complications: Insights into Preeclampsia and Gestational Diabetes Mellitus. Current Issues in Molecular Biology 2025, Vol 47, Page 685 47:685. https://doi.org/10.3390/CIMB47090685

14. Phillips AK, Roy SC, Lundberg R, et al (2014) Neonatal iron status is impaired by maternal obesity and excessive weight gain during pregnancy. Journal of Perinatology 34:513–518. https://doi.org/10.1038/jp.2014.42

15. Kopeć Z, Starzyński RR, Jończy A, et al (2021) Role of Iron Metabolism-Related Genes in Prenatal Development: Insights from Mouse Transgenic Models. Genes (Basel) 12:. https://doi.org/10.3390/GENES12091382

16. Toth IH, Pantea MM, Enatescu I, et al (2026) Umbilical Cord Biomarkers of Nutritional and Metabolic Status in Neonates with Intrauterine Growth Restriction. J Clin Med 15:. https://doi.org/10.3390/JCM15031043

17. McCarthy EK, Murray DM, Kiely ME (2022) Iron deficiency during the first 1000 days of life: are we doing enough to protect the developing brain? Proceedings of the Nutrition Society 81:108–118. https://doi.org/10.1017/S0029665121002858

18. Fisher AL, Nemeth E (2017) Iron homeostasis during pregnancy. Am J Clin Nutr 106:1567S-1574S. https://doi.org/10.3945/ajcn.117.155812

19. Mégier C, Peoc'h K, Puy V, Cordier AG (2022) Iron Metabolism in Normal and Pathological Pregnancies and Fetal Consequences. Metabolites 12

20. O'Brien K, Wang Y (2023) The Placenta: A Maternofetal Interface. Annu Rev Nutr 43:301–325. https://doi.org/10.1146/ANNUREV-NUTR-061121-085246

21. Sangkhae V, Fisher AL, Ganz T, Nemeth E (2023) Iron Homeostasis During Pregnancy: Maternal, Placental, and Fetal Regulatory Mechanisms. Annu Rev Nutr 43:279–300. https://doi.org/10.1146/ANNUREV-NUTR-061021-030404

22. Koenig MD, Tussing-humphreys L, Day J, et al (2014) Hepcidin and Iron Homeostasis during Pregnancy. 3062–3083. https://doi.org/10.3390/nu6083062

23. Zhao Z, Shi Y, Sun M, Wang B (2025) Effects of prenatal iron deficiency on neurological development and related disorders in offspring. Front Nutr 12:. https://doi.org/10.3389/FNUT.2025.1637398

24. Behariera O, Kajiwarab K, Sadovskyb Y, et al (2021) Ferroptosis, trophoblast lipotoxic damage, and adverse pregnancy outcome. Placenta 108:32–38. https://doi.org/10.1016/j.placenta.2021.03.007

25. Zhang Y, Lu Y, Jin L (2022) Iron Metabolism and Ferroptosis in Physiological and Pathological Pregnancy. Multidisciplinary Digital Publishing Institute

26. Shen X, Obore N, Wang Y, et al (2023) The Role of Ferroptosis in Placental-Related Diseases. Reproductive Sciences 2023 30:7 30:2079–2086. https://doi.org/10.1007/S43032-023-01193-0

27. Ng S-KKW, Lee C, Ng AC, et al (2023) Ferroportin expression and regulation in human placenta/fetal membranes: Implications for ferroptosis and adverse pregnancy outcomes. Elsevier

28. Lean SC, Candia AA, Gulacsi E, et al (2022) Obesogenic diet in mice compromises maternal metabolic physiology and lactation ability leading to reductions in neonatal viability. Acta Physiologica 236:1–22. https://doi.org/10.1111/apha.13861

29. Riemer J, Hoepken HH, Czerwinska H, et al (2004) Colorimetric ferrozine-based assay for the quantitation of iron in cultured cells. Anal Biochem 331:370–375. https://doi.org/10.1016/j.ab.2004.03.049

30. Clercq K De, Lopez-Tello J, Vriens J, et al (2020) Double-label immunohistochemistry to assess labyrinth structure of the mouse placenta with stereology. Placenta 94:44–47. https://doi.org/10.1016/j.placenta.2020.03.014

31. Bankhead P, Loughrey MB, Fernández JA, et al (2017) QuPath: Open source software for digital pathology image analysis. Scientific Reports 2017 7:1 7:1–7. https://doi.org/10.1038/s41598-017-17204-5

32. Vandesompele J, De Preter K, Pattyn F, et al (2002) Accurate normalization of real-time quantitative RT-PCR data by geometric averaging of multiple internal control genes. Genome Biology 2002 3:7 3:research0034.1-. https://doi.org/10.1186/GB-2002-3-7-RESEARCH0034

33. Andersen CL, Jensen JL, Ørntoft TF (2004) Normalization of Real-Time Quantitative Reverse Transcription-PCR Data: A Model-Based Variance Estimation Approach to Identify Genes Suited for Normalization, Applied to Bladder and Colon Cancer Data Sets. Cancer Res 64:5245–5250. https://doi.org/10.1158/0008-5472.CAN-04-0496

34. Pfaffl MW, Tichopad A, Prgomet C, Neuvians TP (2004) Determination of stable housekeeping genes, differentially regulated target genes and sample integrity: BestKeeper - Excel-based tool using pair-wise correlations. Biotechnol Lett 26:509–515. https://doi.org/10.1023/B:BILE.0000019559.84305.47/METRICS

35. Marsh B, Blelloch R (2020) Single nuclei RNA-seq of mouse placental labyrinth development. Elife 9:1–27. https://doi.org/10.7554/ELIFE.60266

36. Jones AD, Zhao G, Jiang YP, et al (2016) Maternal obesity during pregnancy is negatively associated with maternal and neonatal iron status. Nature Publishing Group

37. Jones AD, Shi Z, Lambrecht NJ, et al (2021) Maternal Overweight and Obesity during Pregnancy Are Associated with Neonatal, but Not Maternal, Hepcidin Concentrations.

38. Dao MC, Sen S, Iyer C, et al (2012) Obesity during Pregnancy and Fetal Iron Status: is Hepcidin the link? Journal of Perinatology 33:177–181. https://doi.org/10.1038/jp.2012.81

39. Tang D, Chen X, Kang R, Kroemer G (2020) Ferroptosis: molecular mechanisms and health implications. Cell Research 2020 31:2 31:107–125. https://doi.org/10.1038/s41422-020-00441-1

40. Georgieff MK (2011) Long-term brain and behavioral consequences of early iron deficiency. Nutr Rev 69:S43–S48. https://doi.org/10.1111/J.1753-4887.2011.00432.X

41. Georgieff MK (2023) The importance of iron deficiency in pregnancy on fetal, neonatal, and infant neurodevelopmental outcomes. International Journal of Gynecology and Obstetrics 162:83–88. https://doi.org/10.1002/IJGO.14951

42. Fretham SJB, Carlson ES, Georgieff MK (2011) The Role of Iron in Learning and Memory. Advances in Nutrition 2:112–121. https://doi.org/10.3945/AN.110.000190

43. Lozoff B, Beard J, Connor J, et al Long-Lasting Neural and Behavioral Effects of Iron Deficiency in Infancy. Nutr Rev 64:S34–S43. https://doi.org/10.1111/J.1753-4887.2006.TB00243.X

44. Radlowski EC, Johnson RW (2013) Perinatal iron deficiency and neurocognitive development. Front Hum Neurosci 7:56184. https://doi.org/10.3389/FNHUM.2013.00585/TEXT

45. Barks AK, Fretham SJBB, Georgieff MK, Tran P V. (2018) Early-Life Neuronal-Specific Iron Deficiency Alters the Adult Mouse Hippocampal Transcriptome. Elsevier

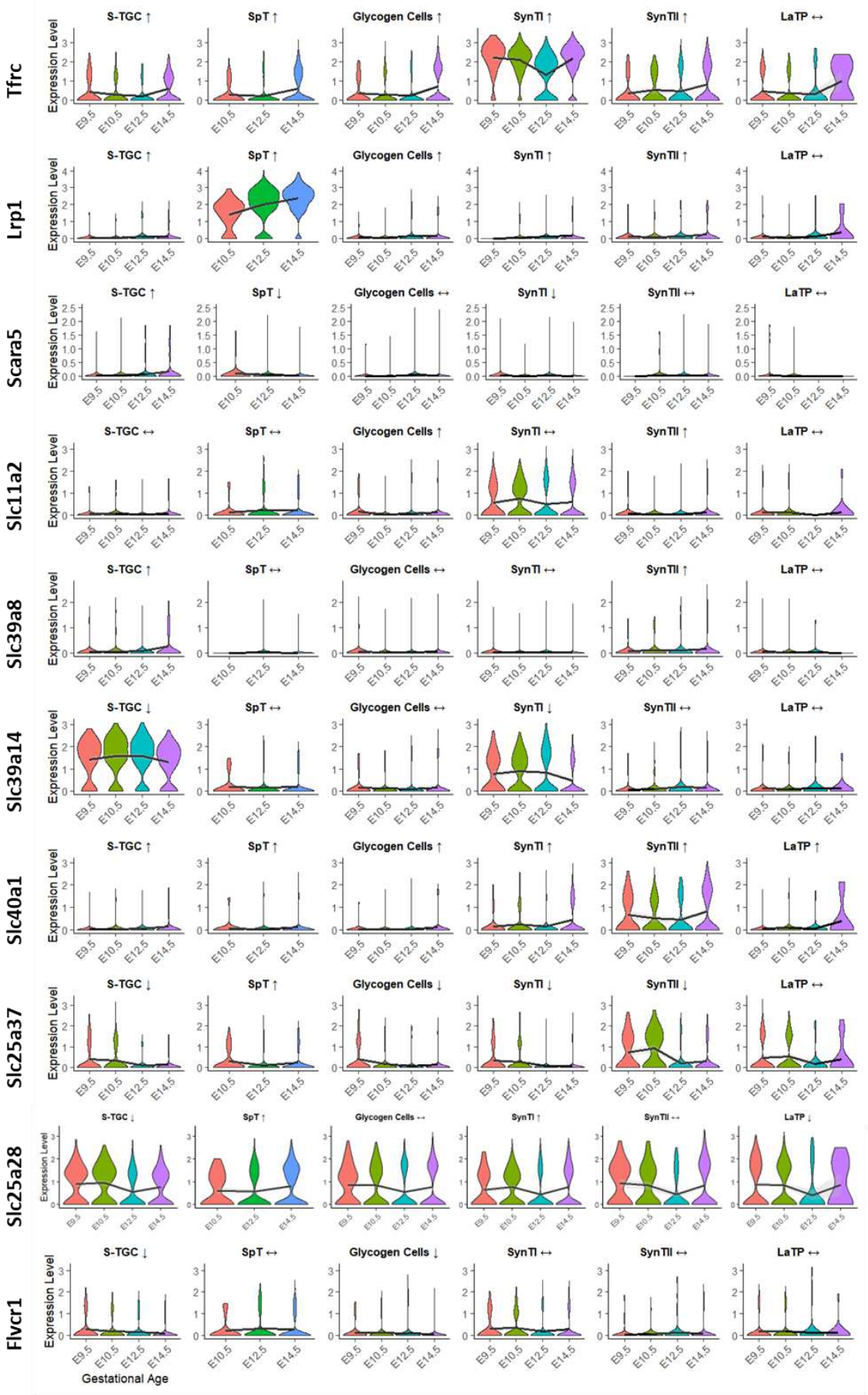
46. Qiu L, Frazer DM, Hu M, et al (2025) Mechanism and regulation of iron absorption throughout the life cycle. J Adv Res 77:107–118. https://doi.org/10.1016/J.JARE.2025.01.002

47. Alwan NA, Hamamy H (2015) Maternal Iron Status in Pregnancy and Long-Term Health Outcomes in the Offspring. J Pediatr Genet 4:111. https://doi.org/10.1055/S-0035-1556742

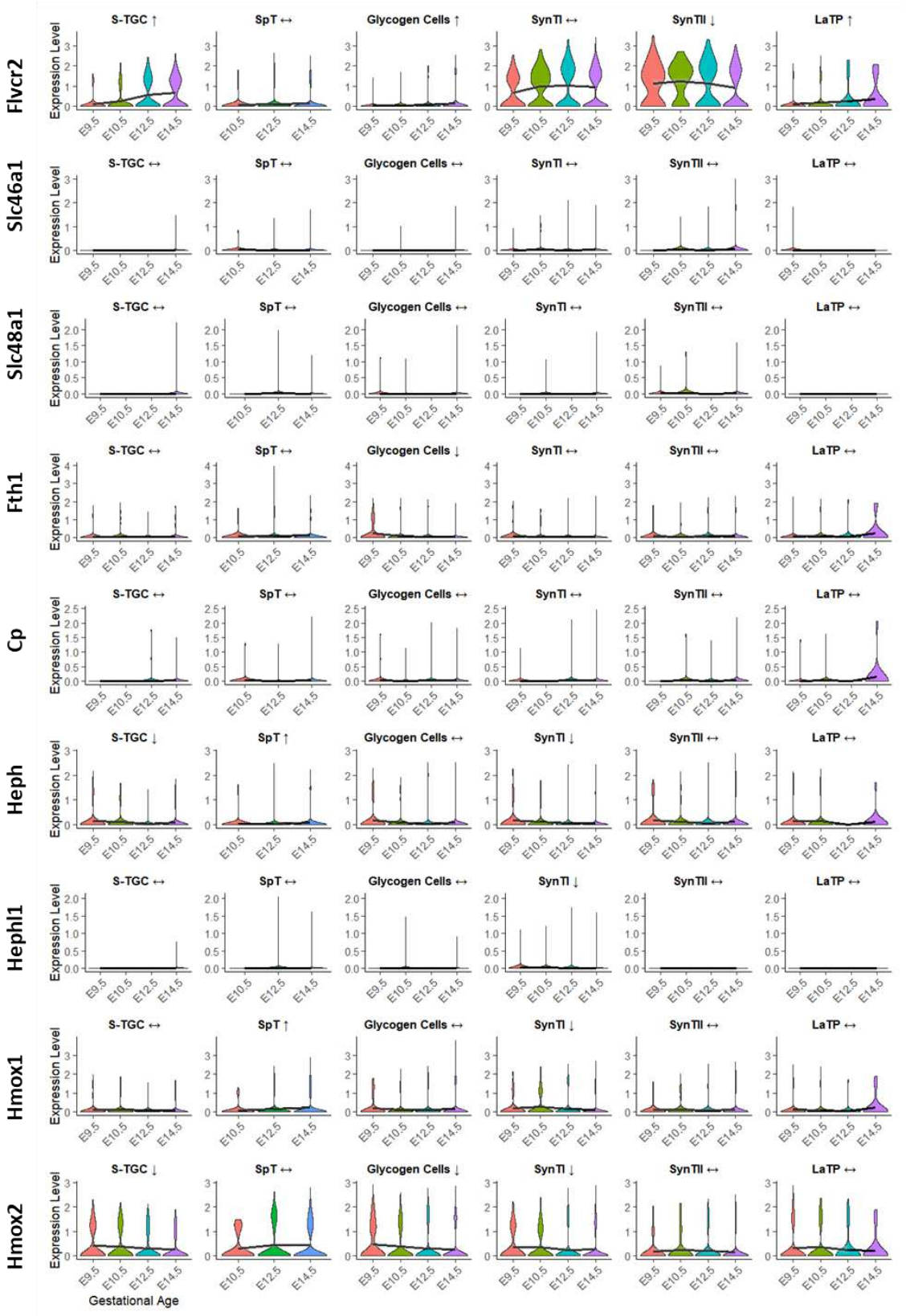
48. Bahr TM, Benson AE, Kling PJ, et al (2021) Maternal obesity and impaired offspring neurodevelopment: could fetal iron deficiency be a pathogenic link? J Perinatol 41:1199–1200. https://doi.org/10.1038/S41372-021-00951-9

49. Schroeder M, Yi N, Fuenzalida B, et al (2026) Placental iron transport under maternal stress: a missing link in foetal programming and mental health. EBioMedicine 125:. https://doi.org/10.1016/j.ebiom.2026.106170

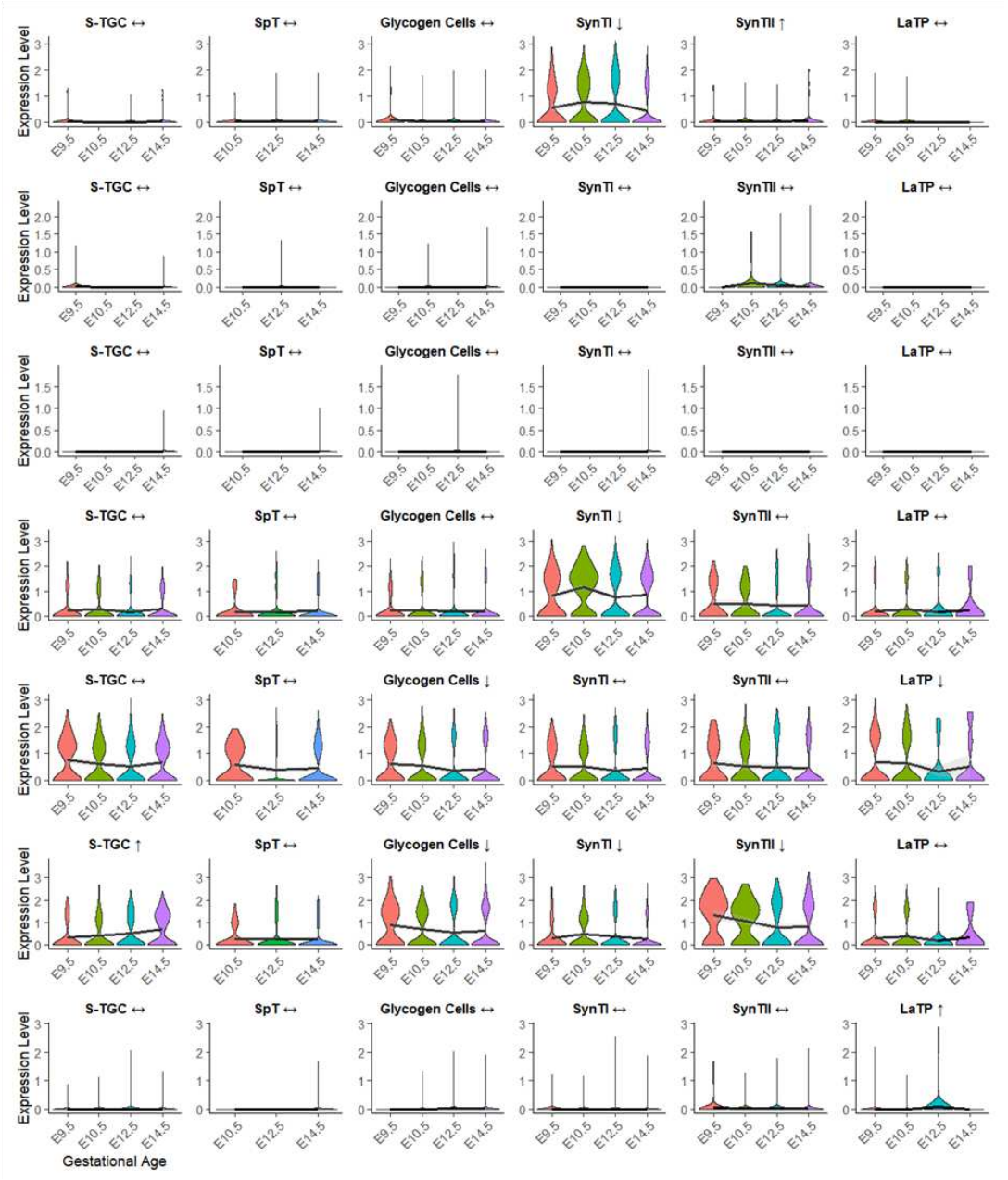
8 Supplemental material



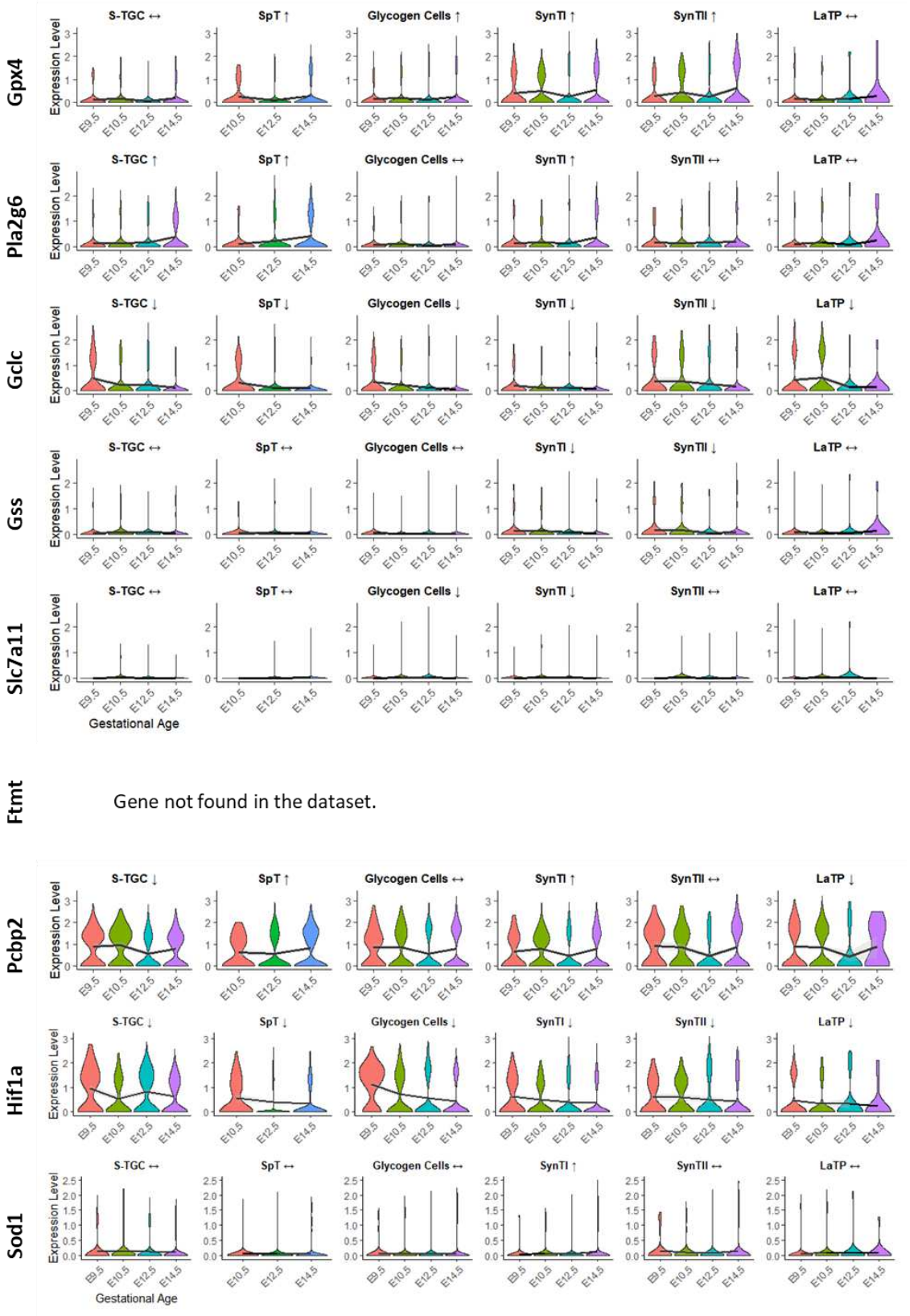
Suppl. Figure 1: Temporal expression of iron homeostasis gene and ferroptosis marker across trophoblast cell lineages during mouse placental development.



Suppl. Figure 1 (continued): Temporal expression of iron homeostasis gene and ferroptosis marker across trophoblast cell lineages during mouse placental development.


Steap3
Hamp
Hfe
Aco1
Ireb2
Acsl4
Dpp4
Alox15
Aifm2
S-TGC ↔
SpT ↔
Glycogen Cells ↔
SynTI ↓
SynTII ↑
LaTP ↔
Expression Level
E9.5
E10.5
E12.5
E14.5
Gestational Age
Gene not found in the dataset.

Suppl. Figure 1 (continued): Temporal expression of iron homeostasis gene and ferroptosis marker across trophoblast cell lineages during mouse placental development.



Suppl. Figure 1 (continued): Temporal expression of iron homeostasis gene and ferroptosis marker across trophoblast cell lineages during mouse placental development.

Legend: Violin plots show gene expression distribution in six trophoblast cell populations across gestational timepoints (E9.5-E12.5). Black lines represent mean expression values with gray shaded areas indicating 95% confidence intervals. Symbols in plot titles denote significant trends in expression over time (↑: significant increase, ↓: significant decrease, ↔: no significant trend,

887 $p<0.05$). The analysis reveals distinct temporal regulation of Slc48a1 across different trophoblast subtypes, suggesting cell-type
888 specific roles in placental iron metabolism during development. S-TGC: sinusoidal trophoblast giant cells; SpT: spongiotrophoblast;
889 SynTI/II: syncytiotrophoblast layers I and II; LaTP: labyrinth trophoblast progenitors.

Supplementary Files

This is a list of supplementary files associated with this preprint. Click to download.

- JMMeKeyMessages.docx
- Suppl.Figure1continued1.png
- Suppl.Figure1continued2.png
- Suppl.Figure1continued3.png
- Suppl.Figure1.png